EI 109

ACTA POLYTECHNICA SCANDINAVICA

ELECTRICAL ENGINEERING SERIES No. 109

A Calculable Impulse Voltage Calibrator

JARI HÄLLSTRÖM

Helsinki University of Technology
High Voltage Institute
P.O. Box 3000
FIN-02015 HUT
FINLAND

Dissertation for the degree of Doctor of Science in Technology to be presented with due permission of the Department of Electrical and Communications Engineering for public examination and debate in Auditorium S4 at Helsinki University of Technology (Espoo, Finland) on the 1st of November, 2002, at 12 noon.

ESPOO 2002

Hällström, J. **A Calculable Impulse Voltage Calibrator**, Acta Polytechnica Scandinavica, Electrical Engineering Series No. 109, Espoo 2002, 107 p. Published by the Finnish Academies of Technology.

ISBN 951-666-609-4, ISSN 0001-6845 (print)
ISBN 951-22-6174-X (pdf)

Keywords: High voltage, impulse voltage, calibration

Abstract

This thesis describes the principle, design, construction, and uncertainty analysis of a calculable impulse voltage calibrator. The calibrator can be used as a primary reference for impulse voltage measurements. The calibrator generates lightning impulses (LI) with known peak value (U_P), front time (T_1), and time to half value (T_2); or switching impulses (SI) with known peak value (U_P), time to peak (T_P), and time to half value (T_2). The peak voltages of the constructed devices range from 50 mV to 1000 V.

The calibration of impulse voltage measuring equipment is required both by high voltage and quality standards, and the gap between the best measurement accuracy available at National Metrology Institutes; the accuracy that is required in high voltage testing has been very narrow. The only way to improve the situation is to lower the measurement uncertainty levels in the National Metrology Institutes.

In this work, the traceability of the peak and time parameter values is based on the modelling of the circuit, and the calculation of these parameters according to network theory. This calculation is based on the calibrated component (resistor and capacitor) values of the impulse circuit. The uncertainty in the peak values is low, as the peak value is not sensitive to changes in the component values of the circuit.

The estimated uncertainties for lightning impulse calibrators are 0,05% for peak value, 0,5% for front time, and 0,3% for time to half value. For switching impulses the corresponding uncertainties are 0,1%, 0,4% and 0,3%.

The calibrators based on this work have been used for calibration work at Helsinki University of Technology, and as a transfer reference in an ongoing worldwide round-robin test.

© All rights reserved. No part of the publication may be reproduced, stored in a retrieval system, or transmitted, in any form or by any means, electronic, mechanical, photocopying, recording, or otherwise, without the prior permission of the author.

“…

And what can I do if life
appears to be a big poem,
for which the Creator gave us threads
and gave us a command: weave!

We weave from the cradle to our
grave, we weave and ravel again,
until death will break our song,
and we’ll take it back to its tuner.

Who carries a wise conclusion,
who sketched a caricature,
who has some small poems with him,
who carries an heroic epic.

But whether it’s a mood, an epigram
or a reflection of great depth,
all poems are good for the Creator,
if the poem is fine and right.

…”

Eino Leino

Singer’s song
(from “Hundred and one songs”, 1898)

“…

Ja minkä mä taidan, jos elämä tää
vain mulle on suuri runo,
mihin saimme me Luojalta langat vaan
ja Luojalta käskyn: puno!

Me punomme kehdosta hautahan,
me punomme, puramme jälleen,
kunis laulumme kuolema katkaisee
ja sen viemme me virittäjälleen.

Kuka viepi viisahan päätelmän,
kuka piirteli pilkkataulun,
kenen pivoss’ on pieniä runoja vaan,
kenen kädessä sankarilaulu.

Mut olkoon se tunnelma, kompa vaan
tai miehen mietelmä syvä,
runot kaikki Luojalle kelpaavat,
jos runo on muuten hyvä.

…”

Eino Leino

Laulajan laulu
(kokoelmasta ”Sata ja yksi laulua”, 1898)

Preface

This work was carried out at the High Voltage Institute of Helsinki University of Technology (HUT) during the years 1991-2001. Although this doctoral thesis is a monograph, some of the material is based on papers presented earlier [1-4].

Aro and Rantanen first published the idea of a calculable calibrator, which produces a lightning impulse of known peak value, in 1979 [5]. In 1991, a project was started at the High Voltage Institute (HVI) aiming to achieve the status of a National Metrology Institute. As a part of that larger project, the idea of a calculable impulse voltage calibrator arose. The author improved the initial design, and extended the idea to cover time parameters. HVI achieved National Metrology Institute status in 1994.

As a continuation of earlier intercomparison projects coordinated by HUT, a worldwide round robin project for LI and SI measurements started in 1998. This project is financed by the Standards, Measurements, and Testing Programme of the Commission of the European Community. As part of this project, the accuracy of the calculable impulse voltage calibrator was further improved, and a new calibrator was designed and constructed. This calibrator forms a key part of a transfer reference system being circulated in major National Metrology Institutes and certain accredited and testing high voltage laboratories around the world. Altogether 26 laboratories, of which 15 are outside the European Community, participate in this large-scale exercise.

Up to the end of 2001, five calibrator systems had been built. The first two systems were built in 1999. One of them has been used as the national reference in Finland, and the other as a transfer reference in a large worldwide intercomparison mentioned above. The third system was built in 2001 for a planned bilateral comparison, and it will be used as a transfer reference. Two systems were sold in 2000.

Acknowledgements

I would like to thank my supervisor, Professor Martti Aro, Director of the HVI, for introducing the subject to me and arranging the funding for this work. M.Sc. Mika Kivelä and M.Sc. Hans Karlsson helped me with the construction of the initial designs in the early 1990's. M.Sc. Yuri Chekurov did excellent work in assembling the latest version used for the worldwide comparison.

The worldwide comparison project has produced a flood of measurement results from the participants all over the world. I present thanks to all researchers taking part in this project. In the analysis of these results, the help from M.Sc. Marja-Leena Pykälä has been valuable.

The financial support from the Academy of Finland (Graduate School of Electric Engineering) for writing this thesis is thankfully appreciated.

And finally the warmest thanks my wife Suvi and my sons, Lassi and Jussi, for their love and patience during the years this work has been going on.

I take all responsibility for the possible clumsiness of the translation of the poem on the preceding page; I found it a difficult yet challenging task to try to convey Eino Leino's thoughts to the non-Finnish readers of this thesis.

Espoo, Finland, 2.10.2002 Jari Hällström

The author's contribution

The author has derived the algorithms described in sections 5.1 and 6.2 for the calculation of the impulse parameters. The author is also responsible for the development of the computer program described in section 0 for calculating the parameters according to these formulae.

Design of the calibrator heads described in sections 5.2 and 6.3, as well as that of the system required to run them described in section 4, were performed by the author. The author performed the analyses of uncertainties presented in sections 5.3, 6.4, and Appendix B.

The calibrator system described in this thesis is used as a transfer reference in a worldwide intercomparison project. The author has been responsible for the design and construction of the intercomparison system and, as by-product, of the integration of the calculable calibrator as part of that system.

The results presented in examples 1, 3, and 4 of Chapter 7 are retrieved from the intercomparison project. The author has been responsible for collecting the results from the participants and analysing them.

Table of contents

List of figures

List of tables

List of abbreviations

A/D	Analog-to-digital (converter)
BIPM	International Bureau of Weights and Measures (Bureau International des Poids et Mesures)
BNC	Baby N-connector
CIGRE	International Council on Large Electric Systems (Conférence Internationale des Grands Réseaux Électriques)
CSIRO	Commonwealth Scientific & Industrial Research Organisation (Australia)
DMM	Digital multimeter
DUC	Device under calibration
DUT	Device under test
DVS	Direct voltage source
EA	European co-operation for Accreditation
EMC	Electromagnetic compatibility
f.s.d.	Full scale deflection
FET	Field effect transistor
GUM	Guide to the expression of uncertainty in measurement
HUT	Helsinki University of Technology (Finland)
HVI	High voltage institute
IEC	International Electrotechnical Commission
IEEE	The Institute of Electrical and Electronics Engineers, Inc.
IEEE-488	IEEE standard for instrumentation bus
IGBT	Insulated gate bipolar transistor
ILAC	The International Laboratory Accreditation Cooperation
LI	Lightning impulse

MOSFET	Metal oxide semiconductor field effect transistor
NMI	National Metrology Institute
NPO	Negative positive zero (Unofficial temperature coefficient designation for capacitors)
NRC	National Research Council (Ottawa, Canada)
PCB	Printed circuit board
ppm	part(s) per million
PTB	Physikalisch-Technische Bundesanstalt (Germany)
r.m.s.	Root mean square
RMO	Regional metrology organisation
SI	Switching impulse
SI	The international system of units (Système International d'Unités)
SMD	Surface mount device
TCR	Temperature coefficient of resistance
WG	Working group
VNIIMS	All-Russian Institute of Metrological Service

List of symbols

α	angle
φ	angle
π	pi (≈3,14159)
τ	time constant
a, b, c, d	coefficients of a polynomial
C_1	capacitor
C_B (C_F)	front capacitor of a Marx generator circuit
C'_B	parallel connection of C_B and C_L (Change C'_B with C_B ?)
C_D	damping capacitor
C_{IN}	input capacitance of the device under calibration
C_L	load capacitance for impulse calibrator
C_S (C_T)	tail capacitor of a Marx generator circuit
C'_S	distributed tail capacitor of a Marx generator circuit
D	determinant
f_R	resonant frequency
G	sphere gap
g, h	roots of a second degree polynomial
I_1, I_2, I_3	loop currents in a Marx generator circuit
J_1, J_2	shorting links
k	level of uncertainty
L_S	stray inductance
n	number of stages in Marx generator
N	number of observations
p, q	coefficients of a polynomial
R_A, R_B, R_1, R_2	resistors
R_C	charge current limiting resistor
R'_C	distributed charge current limiting resistor

R_D (R_F)	front resistor of a Marx generator circuit
R'_D	distributed front resistor of a Marx generator circuit
R''_D	distributed front resistor of a Marx generator circuit
R_E, (R_T)	tail resistor of a Marx generator circuit
R'_E	distributed tail resistor of a Marx generator circuit
R_{IN}	input resistance of the device under calibration
R_L	load capacitance for impulse calibrator
S_1, S_2	relay or switch
s	Laplace domain variable $s = j\omega$
s_1, s_2, s_3, s_n	roots of a polynomial of s
t	time
t_{30}	the time on the front of an impulse when it crosses 30% of its peak value
t_{50}	the time on the tail of an impulse when it crosses 50% of its peak value
t_{90}	the time on the front of an impulse when it crosses 90% of its peak value
t_i	time at the ith iteration of the Newton method
t_p	time from the onset of an impulse to its peak value
T	rise time from 30% to 90%
T'	time from virtual origin to 30% level of a lightning impulse
T_1	front time of a lightning impulse (IEC 60060-1), 1,67 T
T_2	time to half-value of a lightning or switching impulse (IEC 60060-1)
T_C	time to chopping of a lightning impulse (IEC 60060-1)
T_d	time above 90% of a switching impulse (IEC 60060-1)
T_P	time to peak of a switching impulse (IEC 60060-1)
U_C	charging voltage for a Marx generator
U_{IN}	input voltage of the device under calibration
u_{comb}	estimated combined uncertainty
u_{std}, u_{hut}, u_{csiro}	estimated uncertainty contributions

$u_O(t)$	output voltage of a calibrator as function of time
$u'_O(t)$	first derivative of $u_O(t)$
$u''_O(t)$	second derivative of $u_O(t)$
$\hat{u}_O$	maximum value of $u_O(t)$
$U_O(s)$	output voltage of a calibrator in frequency (Laplace) domain
U_P	peak value of a lightning or switching impulse (IEC 60060-1)
Z_1, Z_2	Zener diode
z	variable
z_1, z_2, z_3, z_n	roots of a polynomial of z

1 Introduction

This research project has been initiated, and work on it has been performed because of lightning. The components used in electric power transmission and distribution networks are designed to withstand natural lightning overvoltages up to a certain level. To test the capability of these devices to survive lightning strikes, they are tested during manufacture using a "standard lightning impulse". This is a standardised voltage pulse, which is agreed to represent the electrical stress that natural lightning overvoltages present to the equipment. The duration of this transient voltage is some tens of microseconds.

Another source of transients that stress the network components is the opening and closing of switches connecting or disconnecting different sections of the distribution network. These transients, too, have been standardised, and are referred to as "standard switching impulse". The duration of a standard switching impulse is some milliseconds.

During testing, these transients must be measured, and the appropriate measuring equipment calibrated. The calculable impulse calibrator described in this thesis makes the calibration of these instruments more accurate, and clarifies the traceability of the measured quantities.

The main argument for this work is the narrow gap between the accuracy required for the impulse voltage testing and the best calibration accuracy available at the National Metrology Institutes. The solution presented in this work reduces the uncertainty of impulse voltage calibration by approximately one order of magnitude.

The calibrators have proven their applicability in a large-scale comparison project of impulse voltage measuring systems. The project started in 1999, and is still ongoing. The project strives for the highest accuracy of both high and low voltage impulse measurements. The calculable calibrator presented in this thesis is used as a transfer reference device in this worldwide exercise.

1.1 Organisation of the thesis

The organisation of the thesis is as follows: Chapter 2 presents background to the creation and measurement of high impulse voltages. Chapter 3 gives an overview of the standards and literature on calculable impulse voltage calibrators.

Chapter 4 describes the design of the impulse calibration system. Chapter 5 probes into details of a calibrator head designed for calibration of devices with high input impedance. The uncertainty analysis of parameters of the impulses delivered by the calibrator head is also presented. Chapter 6 presents a corresponding description of a calibrator head capable of delivering impulses to lower impedance loads.

Chapter 7 describes four examples of calibrations where the calculable calibrator has been used as a reference device. The results of a comparison with another National Metrology Institute are also presented.

1.2 Calculable impulse voltage calibrator

This thesis describes the design, construction, and verification of a calculable impulse voltage calibrator. It is a single stage impulse generator (see Figure 1), with accurately known component values. When these values and the charging voltage of the circuit are determined, the peak value of the impulse generated by the closing of the switch can be calculated with very high accuracy.

The output waveform is a double exponential curve, whose shape depends on the selection of component values. By appropriate selection of component values, the circuit produces either a standard lightning or switching impulse.

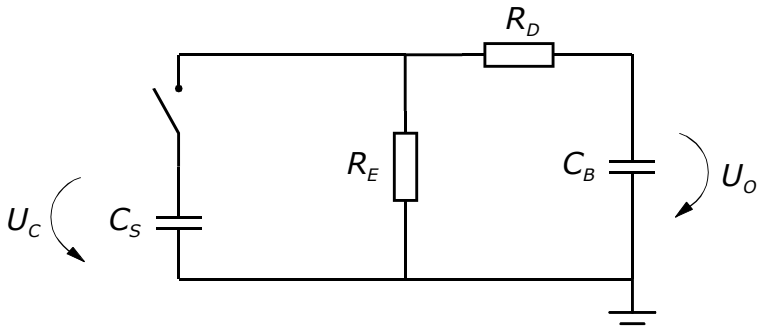

Figure 1 Typical equivalent circuit of a single stage impulse generator.

The solution of the waveform produced by the circuit in Figure 1 can be calculated either by using a circuit simulation program or by solving the circuit equation using the Laplace transform. The latter solution has been studied and used for this project.

It will turn out that the calculated peak value of the impulse is not sensitive to changes in the component values. This means that, for example, if a capacitance value changes by 1%, the peak value will change by only 0,05%. As a

consequence, 0,1% uncertainty in the calculated peak value can in principle be achieved by determining the component values with less than 1% uncertainty. This feature renders the circuit ideal for calibration purposes.

Time parameters (T_1, T_2, T_p, and T_d) can also be retrieved by calculation, but not with as low uncertainty as peak value.

The idea of using a calculated solution of an impulse generator for calibration was originally presented by Aro and Rantanen [5] in 1979. Li, Sheehy and Rungis [6] first introduced the term "calculable impulse voltage calibrator" in 1997.

1.3 Traceability and estimation of uncertainty

This work proposes a new way of providing traceability to impulse voltage measurements. Today's commercial impulse voltage calibrators are based on a stable impulse circuit, and are calibrated using a reference digitiser [7]. The difference of the approach of this thesis compared with current practice in impulse calibrations is shown in Figure 2.

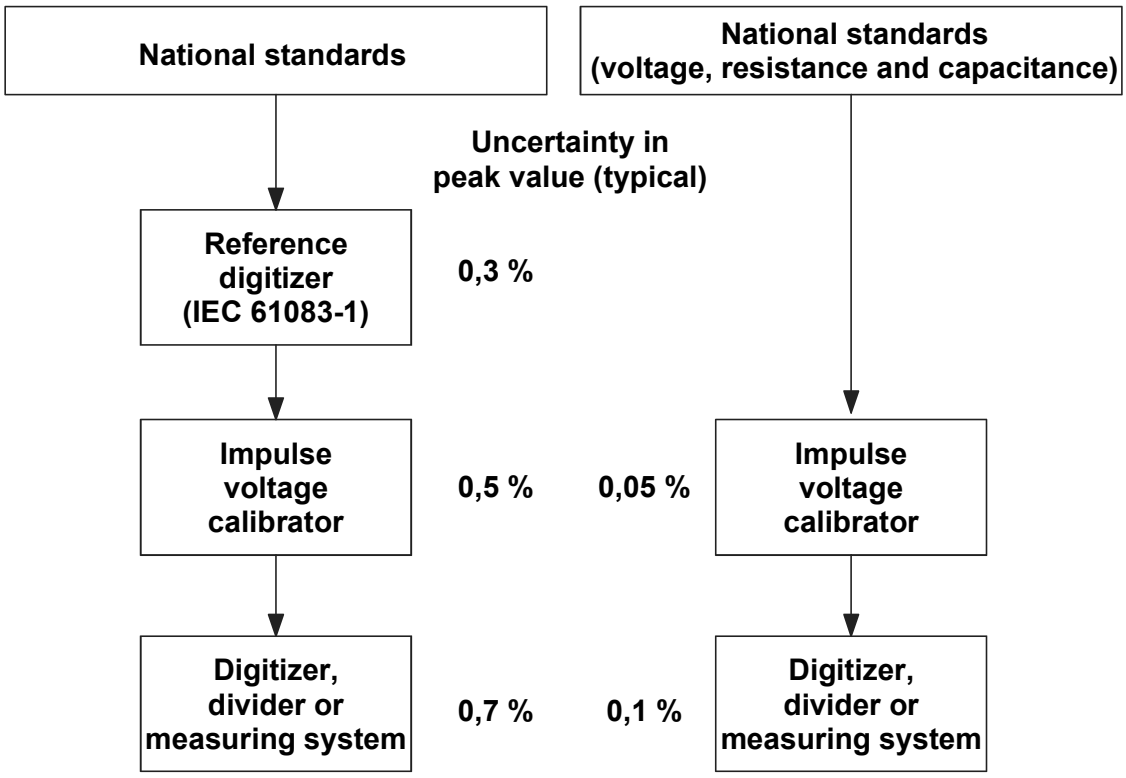

Figure 2 Traceability chain. The current practice shown on the left and the approach used in this work on the right.

The new approach has two advantages over the old one. One step in the reference chain can be omitted, which results in less work and larger margins between each stage in the traceability chain.

The new calibrator additionally presents extremely low uncertainty levels, which cannot be reached using the former approach. The noise level, resolution, and gain accuracy of the current digitisers limit their use as the primary reference.

2 Background

2.1 Creation of high impulse voltages

The most common circuit for creating an impulse voltage consists of two capacitors, two resistors, and a switching element. One of the capacitors, C_S, is charged and then discharged into the pulse forming network of two resistors and the other capacitor. The basic single stage circuit, with components named according to the notation used in German literature, are shown in Figure 1. The symbols used for C_S, C_B, $R_{E,}$ and R_D in the English literature are C_T, C_F, R_T and R_F, respectively.

The use of this circuit becomes increasingly difficult as the charging voltage increases. The problems are related to the switching of very high voltages with spark gaps, the increase of the size of the elements, the need for high direct voltage, and the suppression of corona discharges during the charging period.

Erwin Marx invented a solution to such problems in 1923 in Braunschweig, Germany. His invention charged a set of capacitors in parallel, and connected them in series with spark gaps for their discharge. One possible topology of a multistage impulse voltage generator is shown in Figure 3. Other circuit topologies have also been proposed and used; see for example [8].

The capacitors C_S' are charged through high valued (typically tens of kilo-ohms) resistors R_C'. To create a high voltage impulse, the lowest spark gap is ignited by a spark plug. This transient causes all remaining spark gaps similarly to ignite. Consequently, all capacitors are effectively connected in series and discharged into the low impedance network (typically tens or hundreds of ohms).

2.2 Measurement of high impulse voltages

Impulse voltages are conventionally measured with systems consisting of a voltage divider and a measuring instrument. Voltage dividers are used to reduce the voltage level from tens and hundreds of kilovolts to be in the input voltage range of the measuring instrument, typically some tens or hundreds of volts. The measuring instrument is usually a digital recorder specially designed for impulse capture. The impulse parameters can also be measured by, for example, a general-purpose digital oscilloscope, an analogue oscilloscope using screen capture with a camera, or a peak voltmeter.

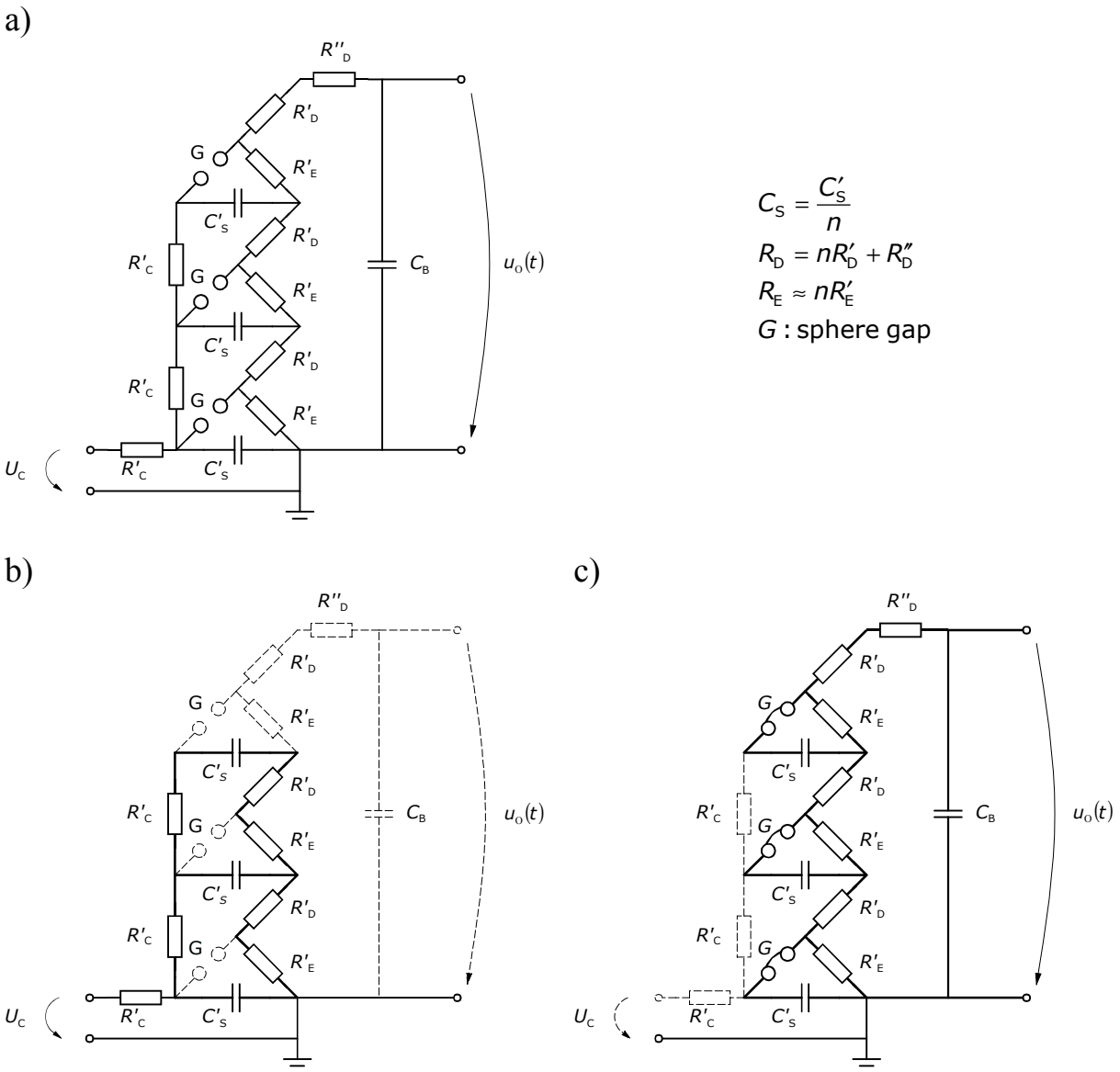

Figure 3 Circuit of a multistage impulse generator (Marx generator).
a) One possible topology,
b) active components during charge, and
c) active components during the discharge of the generator.

The dividers used for capturing a lightning impulse waveform have requirements that are not easy to realise in a single piece of equipment; they should be fast, quickly settling, and should withstand high voltages. The height of the divider is proportional to the required withstand voltage. Typically, the height of these dividers is several meters.

2.3 Traceability and uncertainty

The tradition of requiring a traceable calibration for high voltage measuring systems is not very long. In many European countries, the National Metrology Institutes – formerly National Standard Laboratories – started work on high voltage metrology as late as the 1980s or 1990s.

A guide published by ILAC [9] offers the following definition of traceability:

"Traceability is characterised by a number of essential elements:

- *an unbroken chain of comparisons going back to a standard acceptable to the parties, usually a national or international standard;*
- *measurement uncertainty; the measurement uncertainty for each step in the traceability chain must be calculated according to defined methods and must be stated so that an overall uncertainty for the whole chain may be calculated;*
- *documentation; each step in the chain must be performed according to documented and generally acknowledged procedures; the results must equally be documented;*
- *competence; the laboratories or bodies performing one or more steps in the chain must supply evidence for their technical competence (e.g. by demonstrating that they are accredited);*
- *reference to SI units; the "appropriate" standards must be primary standards for the realisation of the SI units;*
- *recalibrations; calibrations must be repeated at appropriate intervals; the length of these intervals depends on a number of variables, (e.g. uncertainty required, frequency of use, way of use, stability of the equipment)."*

The role of a National Metrology Institute (NMI) is to maintain a national measurement standard, and to verify the correctness of the reference value of the standard and the estimate of its uncertainty by comparison with other NMIs. This principle is clarified in Figure 4.

In order for a reference standard to be accepted, it must be traceable. In the case of the calculable impulse voltage calibrator, the value (resistance, capacitance, or inductance) of each component of the calibrator circuit must be calibrated with known uncertainty.

These values and uncertainties, together with the charging voltage and its uncertainty, are used to calculate the impulse parameters U_P, T_1 or T_P, and T_2. The uncertainty estimate is based on the uncertainties in the component values and charging voltage.

The calibrator described in this work fulfils the requirements set for traceability. The calibrator is used as a national measurement standard for impulse voltages in Finland.

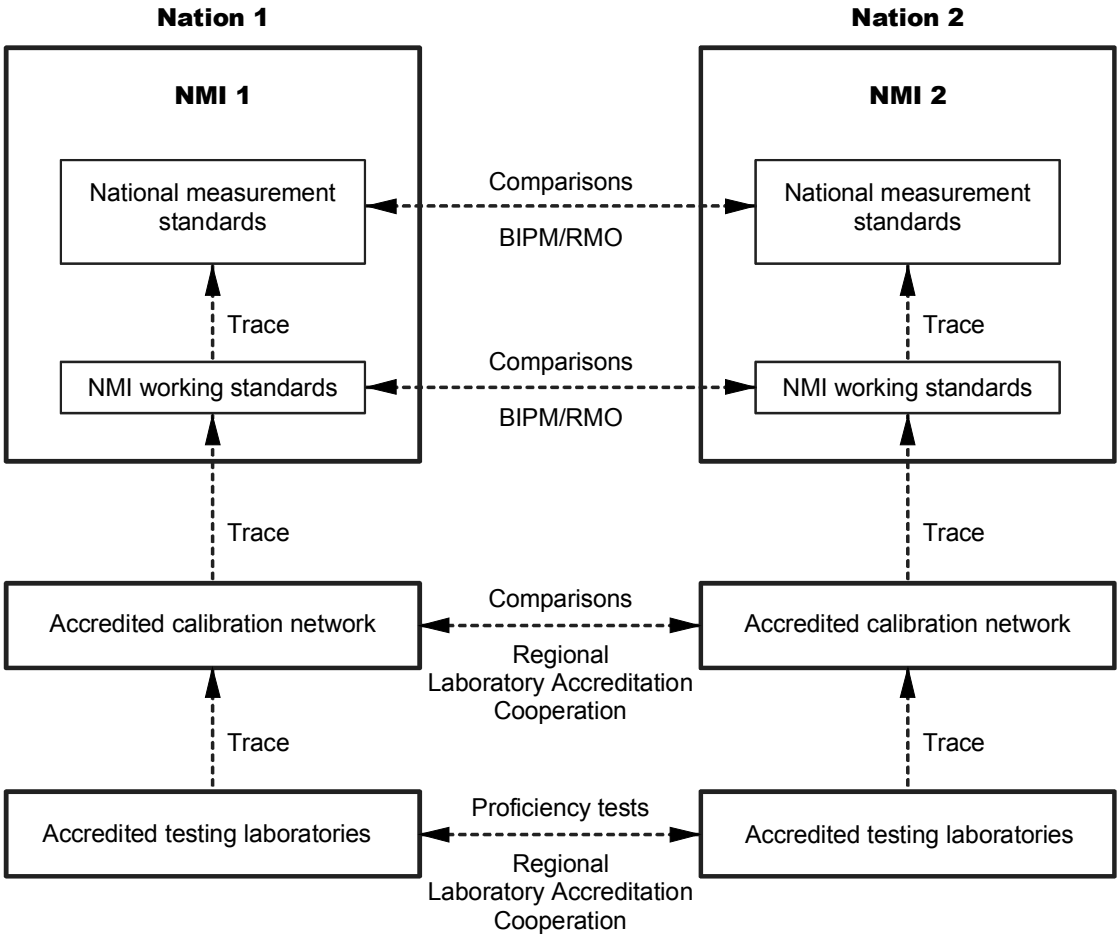

Figure 4 An illustration, for one hypothetical world region, of the complementary roles of the BIPM, the Regional Metrology Organization and the Regional Laboratory Accreditation Cooperation in providing horizontal checks of the equivalence of measurements at various levels of the national calibration hierarchies.
BIPM: Bureau International des Poids et Mesures
NMI: National Metrology Institute.
RMO: Regional Metrology Organization.[10]

3 Standards and literature

3.1 Standards

The quantities measured during impulse voltage tests are defined in standards published by International Electrotechnical Commission (IEC). The relevant IEC standards are listed in Table 1. The IEC 60060 series gives basic definitions for high-voltage quantities. Requirements for the instrumentation and software for high-voltage measuring equipment is given in the IEC 61083 series. The basic EMC publication series IEC 61000 addresses surge immunity tests; the impulses used are almost identical to the lightning and switching impulses defined in IEC 60060-1. This chapter presents a brief summary of the definitions in these standards. The support given for traceable calibration by the standards is also discussed.

Table 1 List of IEC standards related to impulse calibration.

Standard	Name	Connection to this work
IEC 60060-1: 1989 [11]	High-voltage test techniques – Part 1: General definitions and test requirements	- Definition of quantities (U_P, T_1, T_2, T_P ,T_d and T_C)
IEC 60060-2: 1994 [12]	High-voltage test techniques – Part 2: Measuring Systems	- Requirements for *approved measuring systems* and *reference measuring systems*
IEC 61083-1: 2001 [13]	Instruments and software used for measurements in high-voltage impulse tests – Part 1: Requirements for instruments	- Requirements for *reference impulse generators* - Requirements for *approved* and *reference digital recorders*
IEC 61000-4-5: 1995 [14]	Electromagnetic compatibility (EMC) – Part 4: Testing and measurement techniques – Section 5: Surge immunity tests	- Definition of parameters of surges - Requirements for the verification procedure for surge testers

3.1.1 Definitions for lightning impulse

The first edition of IEC 60060 was published in 1938. The definitions of the impulse parameters have remained unchanged at least since the publication of the second edition in 1962.

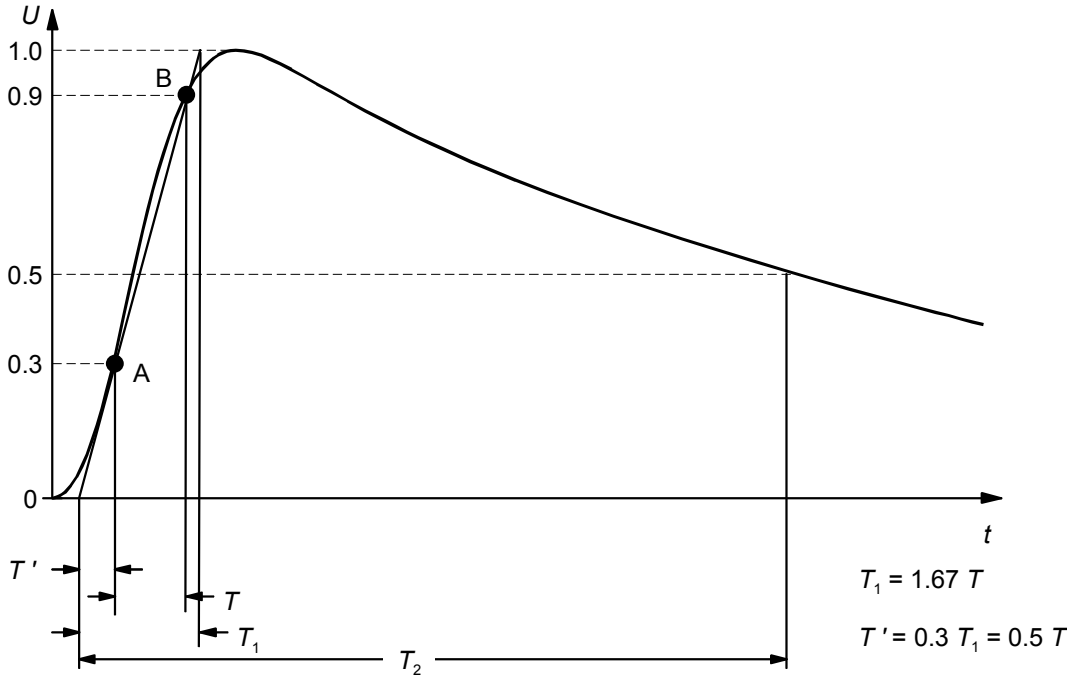

Figure 5 Lightning impulse according to IEC 60060-1. Time scale is not linear.

A normalised full lightning impulse with definitions for time parameters T_1 and T_2 is shown in Figure 5.

The nominal values for T_1 and T_2 are 1,2 µs and 50 µs, respectively. Therefore, the waveform is referred to as a 1,2/50 impulse. However, for practical testing, the parameter values are allowed to differ from the nominal. The standard additionally gives tolerances for the parameters of impulses to be used in testing. The tolerance for T_1 is ± 30% (from 0,84 to 1,56 µs), and for T_2 it is ± 20% (from 40 to 60 µs). The peak value is selected according to the device under test, and its tolerance is ± 3% [11].

The definition of the faster waveform (1,2/50) in the EMC publication IEC 61000-4-5 is taken directly from IEC 60060-1. The slower waveform in that standard uses the same definitions, but the front time is 10 µs and the time to half value 700 µs (10/700).

3.1.1.1 Peak value U_P

The definition of the peak value of the lightning impulse is somewhat ambiguous. The text of the second edition of IEC 60060:1962 [15] requires that

"*if the amplitude of the oscillations is not greater than 5 per cent of the peak value and the frequency is at least 0,5 MHz" [11]*, a mean curve may be drawn for the determination of the peak value. Little guidance is provided for drawing the mean curve. If there are such oscillations on the impulse, as is often the case, the unclear definition causes problems for the evaluation of the parameters.

The same text is copied into subsequent versions, IEC 60060-2:1973 [16] and IEC 60060-1:1989. No references were found, which would clarify the reasons for adapting the 0,5 MHz bandwidth limit for the oscillations to be removed. Certain recent publications suggest that most insulating materials really work that way; they do not see the high-frequency oscillations superimposed on the lightning impulse [17, 18]. However, this interesting subject is beyond the scope of this work.

3.1.1.2 Front time T_1

The front time is defined as *"1,67 times the time interval between the instants when the impulse is 30 per cent and 90 per cent of the peak value"[11]*. Note that T_1 is defined as 1,67 T and not $T/0{,}6$, which would be an accurate translation of the graph in Figure 5. The difference between these is approximately 0,2%. The definition uses 30% level instead of 10 % level to avoid problems with initial distortion caused by the ignition of the spark gaps of the impulse voltage generator.

3.1.1.3 Time to half value T_2

The time to half value is defined as *"the time interval between the virtual origin and the instant on the back (tail), when the voltage has decreased to half the peak value"[11]*. Virtual origin is defined as *"the instant preceding that corresponding to point A by a time 0,3 T_1"[11]*.

3.1.2 Definitions for switching impulse

The switching impulse resembles the lightning impulse in shape, but the main difference is the duration. As the lightning impulse dies out in approximately one hundred microseconds, the switching impulse lasts for some milliseconds. The definitions of switching impulse time parameters are shown Figure 6. The switching impulse was introduced in IEC 60060-2:1973.

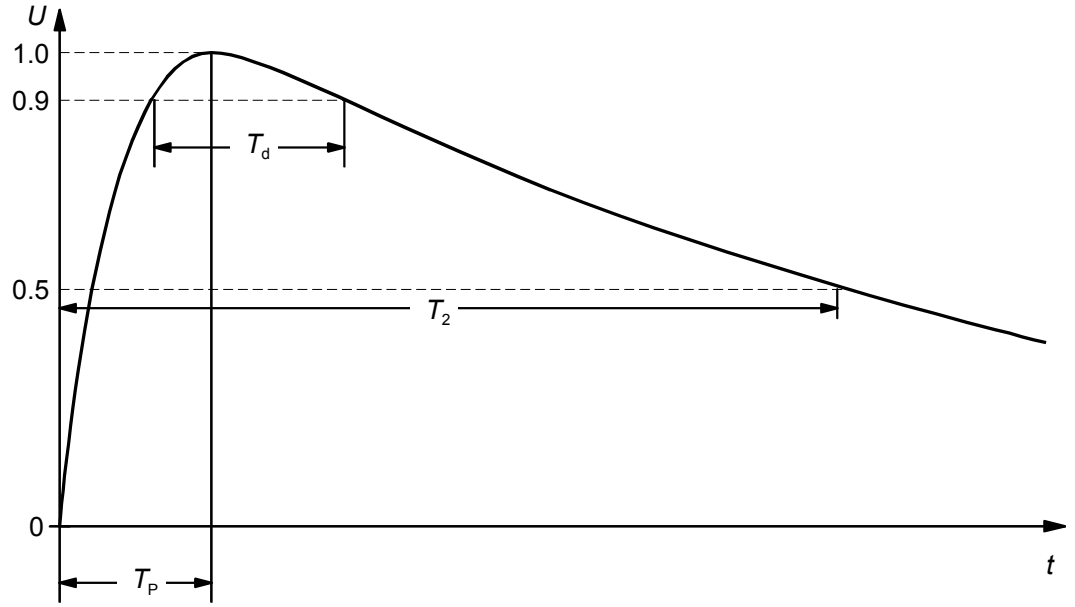

Figure 6 Switching impulse according to IEC 60060-1. Time scale is not linear.

The standard values for the time parameters are 250 μs for time to peak, and 2500 μs for time to half value. The tolerances are ± 20% and ± 60%, respectively. The tolerance for the peak value is ± 3%.

The time parameter definitions are different from those for lightning impulse.

3.1.2.1 Peak value U_P

The value of the test voltage is *"the prospective peak value"* [11].

3.1.2.2 Time above 90% T_d

Time above 90% is *"the time interval during which the impulse voltage exceeds 90% of its peak value"* [11].

3.1.2.3 Time to peak T_P

There is no front time definition for a switching impulse, instead of that the time to peak ("time to crest" in earlier standard editions) was defined as *"the time interval between the actual origin and the instant when the voltage has reached its maximum value"*. The actual origin is now at the beginning of the front of the impulse. The actual origin can be determined from the impulse with good accuracy, but the peak of a switching impulse is flat, and the uncertainty of pointing out the moment of maximum value is large.

3.1.2.4 Time to half value T_2

The time to half value is the "*time interval between the actual origin and the instant when the voltage has first decreased to half the peak value*" [11].

3.1.3 Requirements on calibration

The previous generation of the IEC 60060 family of standards required and gave detailed guidance on verifying the instrumentation using in-house calibrations. Cooperation with national calibration authorities was encouraged but not required.

The major new contribution in IEC 60060-2:1994 was the introduction of *Approved Measuring Systems* and *Reference Measuring Systems*, against which the measuring systems used in tests should be calibrated. This was in line with metrology practices already established in other fields of measurements. Now, the standards give support for preparing these Reference Measuring Systems in National Metrology Institutes and Accredited Calibration Laboratories.

The development of measuring instrument standards reveals a similar tendency. The (now replaced) first version of IEC 60790:1984 [19], *Oscilloscopes and peak voltmeters for impulse tests,* set accuracy requirements and gave guidance on measurements for calibrating the instruments, but did not require traceability for these measurements. The same approach was used in IEC 61083-1:1991, *Digital recorders for measurements in high-voltage tests – Part 1: Requirements for digital recorders*. The current version, IEC 61083-1:2001, *Instruments and software used for measurement in high-voltage impulse tests – Part 1: Requirements for instruments*, adopted the idea of reference measuring systems presented in IEC 60060-2:1994.

3.2 Literature on calculable calibrators

This section presents a review of papers dealing with calculable calibrators. A list of papers published on the subject is presented in Table 2.

During the 1950's and 1960's, several relevant papers were published which dealt with the analytical solution of the impulse generator circuit [20-23]. Such theoretical papers are numerous, and they are not summarised here.

The calculable calibrator is now approximately 20 years old. During the first ten years, three papers were published. The papers presented the first working calibrators and the first verification with an independent method.

Table 2 List of publications on calculable impulse voltage calibrators.

Year	Author(s)	Achievement
1979	M. Aro and Y. Rantanen [5]	- Analysis of sources of uncertainty - Working prototype
1986	M. Aro [24]	- Analytical calculation of U_P in real time using embedded microcomputer
1991	D. Huang, H. Zhou and Y. Zhang [25]	- Comparison between a calculable calibrator and a diode compensation circuit
1993	J. Hällström, M. Aro and M. Kivelä [2]	- Analytical solution for time parameters - Analysis of sources of uncertainty
1994	J.Hällström, M. Aro, V. Kiseliev and V. Jaroslawski [3]	- Comparison between a calculable calibrator, peak comparator, and diode reference
1997	Y. Li, R. Sheehy and J. Rungis [6]	- Alternative design using 50 Ω matching at the end of the cable - Solution using circuit simulator
1998	J. Hällström and M. Aro [4]	- Uncertainty budget - Examples of use
2000	CIGRE Task Force 33.03 3.2 (J. Rungis, R. Hughes, T. McComb, M. Aro, R. Diaz, F. Garnacho, J. Hällström, V. Jaroslawski, J. Kuffel, W. Larzelere, M. Muhr, P. Munhoz Rojas, G. Rizzi, B. Sacepe and K. Schon) [1]	- Presentation of the state of the art - Examples of use
2001	Y. Li, J. Rungis, T.R. McComb and W. Lucas [26]	- Comparison of a calculable calibrator with three reference digitisers

From the beginning of 1990, partly because of new requirements set by IEC standards, more attention was paid to traceability and uncertainty. Results of comparisons with alternative methods were presented. Furthermore, in late 1990´s another research group built a calculable calibrator.

On the first paper published on the subject Aro and Rantanen describe a calibrator capable of producing lightning and switching impulses (1,2/50, 20/2500 and 250/2500) of both polarities [5]. The paper considers only peak value calibration; the time parameters of the generated impulses are not calculated. The sensitivities to changes in component values and in the resistive or capacitive loading of the calibrator are given. The paper points out the fact that relatively large uncertainties in the component values and loading of the

circuit can be allowed without compromising the accuracy of the peak value of the generated impulse. The output voltage peak value was read from tables giving the relation between the charging voltage and peak value for a number of resistive loads. The effect of inductance of the circuit into the calculation was not recognized and it was ignored. The voltage range of the calibrator was from 100 V to 1200 V, and the authors stated an estimated uncertainty of 0,1% for peak value.

Aro published a description of the next version of that calibrator and experience of its use in 1986 [24]. The new calibrator had an embedded microcontroller, which read the charging voltage using an A/D converter and calculated the peak value in real time. The input resistance and capacitance were entered for the peak value calculation by a numeric keypad. This paper concentrates on the properties of the thyristor switch, discussing the voltage drop and the rise time. It further presents results on calibration of a peak voltmeter and an impulse oscilloscope. No estimate for the uncertainty was given. Apart from the embedded microcontroller which made the calibrator considerably more practical, no technical improvements were presented.

In 1991 Huang, Zhou and Zhang published results of a comparison between a diode compensation circuit and the calibrator described in the previous paragraph [25]. They estimated an uncertainty of 0,07% for the diode compensation method, and used a value of 0,2% for the calibrator. The devices agreed within their estimated uncertainties. This was the first independent verification of a calculable calibrator. The publication nicely verified that the idea of a calculable calibrator works.

The author, together with Aro and Kivelä, published a paper describing the analytical solution of the network in detail in 1993 [2]. The paper presented the formulae for calculating the peak value (U_P), the front time (T_1), and the time to half value (T_2). The characteristics of a FET switch used for a new design were presented, as well as results of a calibration of a digitiser. The voltage range was from 100 to 1800 V. The sources of uncertainty contributions were identified and their magnitudes given, but the overall uncertainties were not estimated. The time parameters were now included and the emphasis of the development was shifted on to metrological aspects.

In 1994 a joint work by the author, Aro, Kiseliev and Jaroslawski, three methods for the measurement of the peak value were compared [3]. The calculable calibrator (estimated uncertainty 0,1%) was compared with an electronic dc compensation device (estimated uncertainty 0,1%) [27] and a Zener diode based device (estimated uncertainty 0,05%) [28]. The latter two methods were developed by the All-Russian Institute of Metrological Service (VNIIMS). Both methods agreed with the calibrator within the estimated uncertainties. The systematic differences for the calibrator value were approximately -0,1% for the dc compensation method and approximately +0,1% for the Zener method. The comparison confirmed the uncertainty estimates of all three methods. Only peak voltage measurement was compared, as the methods developed by VNIIMS did not provide information on the time parameters.

During the joint meeting of CIGRE WG33.03 and the IEEE High Voltage Test Technique Group in 1997, the author had a discussion with James McBride from Georgia Institute of Technology, U.S.A. He said that he had used the analytical solution to calculate the peak value of a simple impulse circuit, which he used for the calibration of his lightning impulse measurement equipment. No publication on this work was found.

Li, Sheehy and Rungis from CSIRO, Australia, introduced the term “calculable impulse voltage calibrator” in 1997 [6]. They described a bipolar impulse calibrator for voltages from 6 to 630 V, adding a matching resistor at the end of the connecting cable. This 50 Ω resistor (R_t in Figure 7) acts as a tail resistor and additionally matches the characteristic impedance of the cable. The paper presents the design in detail.

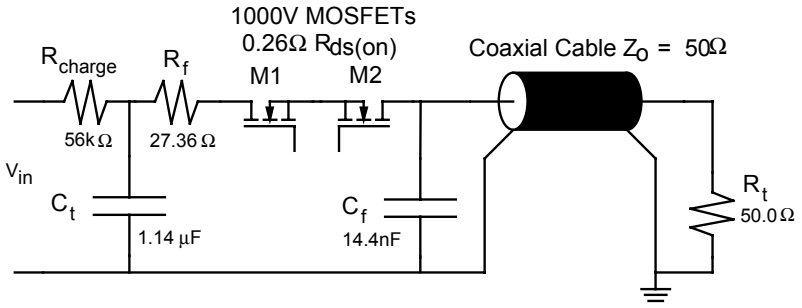

Figure 7 Calculable calibrator design by Li et al. [6].

For the calculation of the impulse parameters, they used commercial circuit simulation software rather than an analytical solution of the network. A detailed analysis of several sources of uncertainty is presented, but no estimate for the overall uncertainty is given. They state that the differences between the calculated values and the values measured with a digitiser match well within the uncertainties specified in IEC standards, if the calibration of the digitiser is considered carefully. This paper presents an independent realisation of a calculable impulse voltage calibrator.

A paper by the CIGRE Working Group 33.03 dealt with the low voltage calibration of high-voltage equipment [1]. This paper included an overview of the impulse calibrators, mainly based on work by the author and Aro from HUT, and Li, Sheehy and Rungis from CSIRO. The paper presents examples on how the calculable calibrator has been used to calibrate measuring instruments and high voltage dividers.

The author and Aro published a paper on the experience with the HUT calibrators in 1998 [4]. In addition to a general discussion on the design, a number of examples of the use of the calibrator were presented. The paper also discusses different types of switches that had been tested during recent years. An uncertainty budget is also available; the estimated uncertainties were 0,08% for U_P, 3,3% for T_1, and 0,5% for T_2.

A joint publication by Li, Rungis, McComb and Lucas published in 2001 compared the CSIRO calibrator with the measuring systems used by CSIRO, NRC and PTB [26]. The estimated expanded uncertainties of the calibrator were 0,1% for peak values, and 1,0% for the time parameters. The corresponding uncertainties for the measuring systems were 0,4 to 0,5% for peak values and 1,0 to 2,0% for the time parameters. In general, the results agree within ±0,5% for U_P, ±2,0% for T_1 and ±1,0% for T_2.

All these publications deal with calibrators of low impedance design.

4 Design principles

4.1 System design

The calibrator system consists of a personal computer (Windows 95 running on a 233 MHz Pentium processor) with IEEE-488 bus, direct voltage source (DVS), digital multimeter (DMM), and a set of calibrator heads. Each calibrator head contains a single stage impulse generator and produces a specific impulse waveshape. Two different designs with different voltage range and load range have been developed. A block diagram of the system is shown Figure 8. A calibrator head is connected to the adapter with a single multiwire cable, and when the calibrator head is changed, only this one must be disconnected. The cables between the adapter, DMM, and DVS are permanently connected. The calibrator head is connected directly to the input of the device under calibration. A typical setup is shown in Figure 9.

The system is controlled by a personal computer, which controls both the charging voltage and digital outputs of the DVS and reads the voltages at the DMM inputs. Impulse is triggered by a signal from the DVS digital outputs. The adapter has the necessary circuitry to adjust the trigger voltage levels for switching elements used for impulse discharging in the calibrator heads.

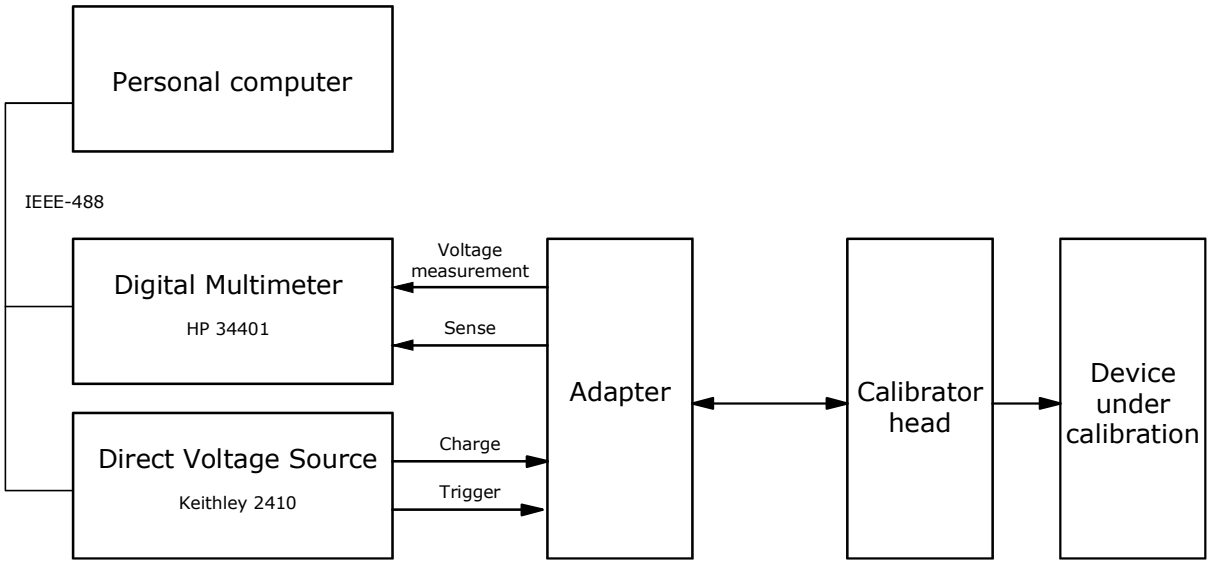

Figure 8 Block diagram showing the components of the calibrator system.

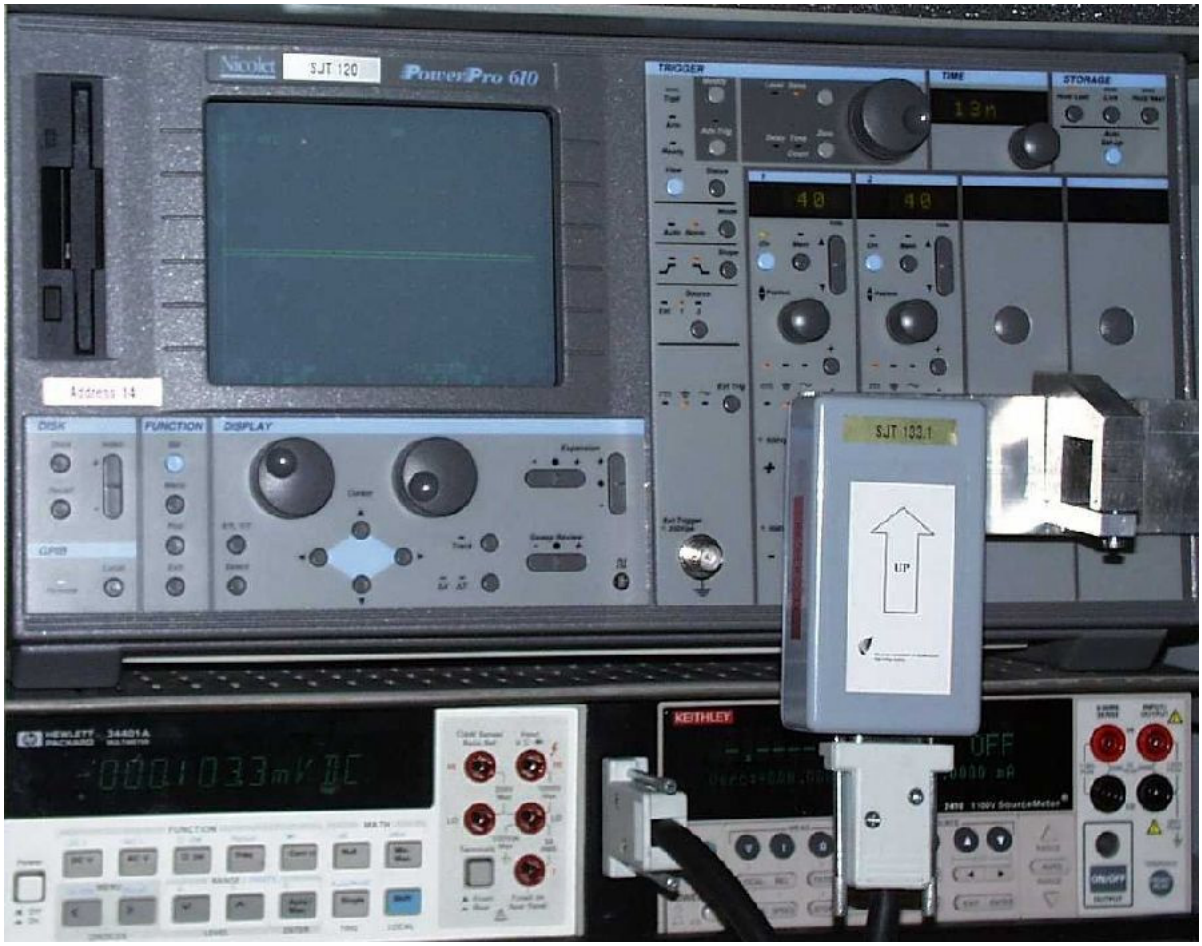

Figure 9 Typical setup of the calibration system. The device under calibration is a digitizer (top). The calibrator head is connected directly to its input. A multiwire cable connects the head to an adapter box (not shown). The adapter is connected to the rear terminals of the direct voltage source (bottom right) and multimeter (bottom left). The controlling computer is not shown.

4.2 Software design

The software has been written using a graphical programming language. The guiding principle in the programming work, as with the entire design of this system, was ease of use. The system was to be sent to a number of high voltage laboratories around the world unaccompanied, and the actual user in the high voltage laboratory should not be worried about the complexity of the calculation. Experience has shown that users have been able to use the software without guidance.

The software is menu based, and guidance on making connections is given on the computer screen, where necessary.

When a calibration is started, the software first detects the calibrator head connected to the system, and loads the respective component values from a file. Other parameters required for calculation (input resistance and capacitance of the device under calibration) are prompted from the user, and their reasonability is checked. The formulae used for calculation are discussed in sections 5.1 and 6.2.

The software shows information on the head currently connected and the parameter values (U_P, T_1/T_P and T_2) of the prospective impulse on screen (see Figure 10). Single impulses or a set of 20 impulses with preset delay can be triggered.

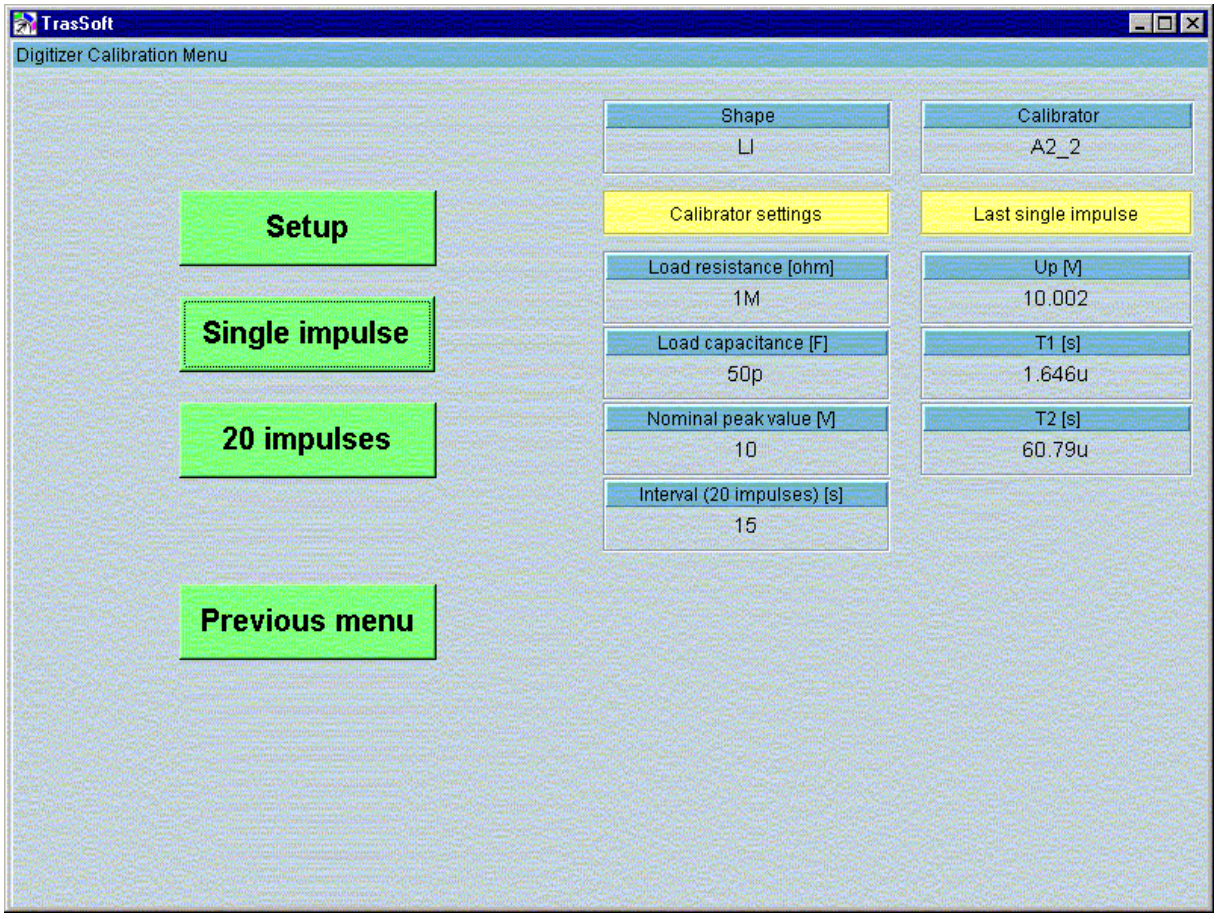

Figure 10 Sample of the calibrator software screen.

Up to now the process of impulse calibration has been automated for two models of digitisers; the software controls both the calibrator and the digitiser and the calibration goes through all the ranges of a digitiser automatically.

At the initialisation stage the software of the personal computer performs the following tasks:

1. Identifies the calibrator head.
2. Loads the parameters of the identified head for U_P, T_1/T_P and T_2 calculations.
3. Prompts the user to key in the input resistance and capacitance of the device under calibration.

After the calibrator head has been identified and the load values keyed in, an impulse can be triggered:

1. The calibrator is charged.
2. The charging voltage of capacitor C_S is measured.
3. The calibrator is triggered.
4. Impulse parameters are evaluated and displayed.

4.2.1 Verification of the calculation

The analytical solution for the impulse generator circuit was studied extensively in the 50s and 60s, before the emergence of modern circuit simulation tools. At that time the best (and the only practical) way to model high voltage impulse generators was to solve the equivalent circuit analytically.

The correctness of the analytical solution and its realisation was checked by comparison. A time domain simulation was carried out for the circuit shown in Figure 12b using circuit simulation software. The component values used for analytical calculation and time domain circuit simulation are shown in Table 3, simulated impulse in Figure 11, and the differences between the parameters calculated by the two methods in Table 4. The good agreement between the analytical solution and circuit simulation verifies the correctness of the solution used in the software.

In the uncertainty analysis the calculation process is disregarded, as contribution from calculation is approximately two orders of magnitude lower than that from the main sources of uncertainty.

Table 3 Comparison between analytical solution and circuit simulation – input parameters.

Input parameters	*Value*
C_S	18,32 nF
C_B	1,2905 nF
R_E	4206,9 Ω
R_D	448,32 Ω
C_L	50 pF
R_L	1 MΩ
U_C	1 V

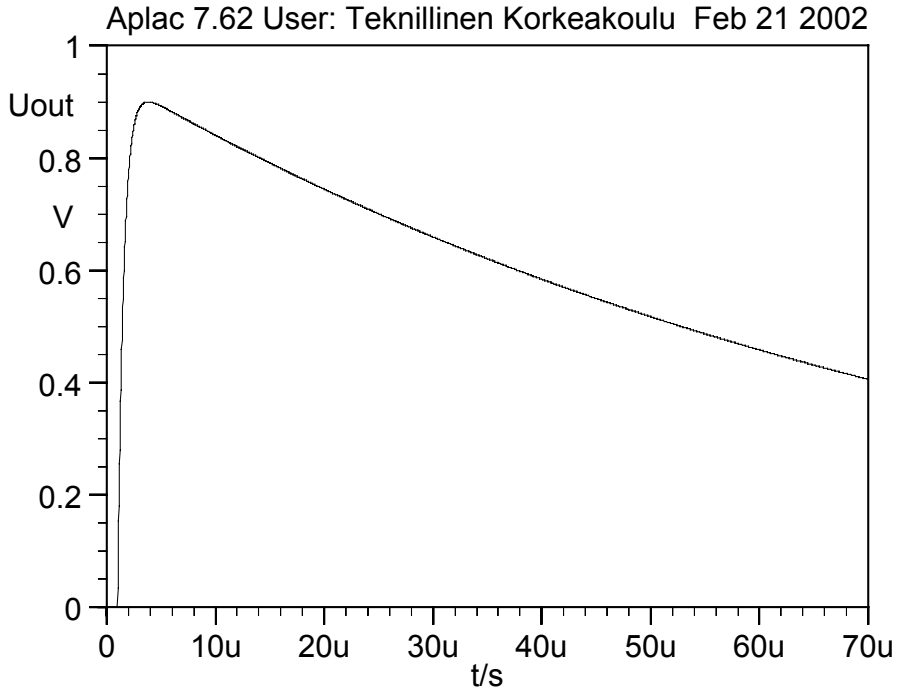

Figure 11 Comparison between analytical solution and circuit simulation – simulated impulse.

Table 4 Comparison between analytical solution and circuit simulation – calculated impulse parameters.

Calculated impulse parameters	*Analytical solution*	*Circuit simulation*	*Difference*
U_p	0,899 753	0,899 75	< 0.0003%
T_1	1,645 899	1,645 96	-0.0037%
T_2	60,789 67	60,789 8	-0.0002%

4.3 Impulse circuit design

4.3.1 Selection of the component values

From the basic circuit theory some rule can be derived for optimising the impulse circuit shown in Figure 1. The rules are approximate, but they give good advice for the selection of component values:

1. The efficiency factor of the circuit is proportional to the ratio of capacitances, C_B/C_S. The efficiency factor is the ratio between the charging voltage and impulse peak value.
2. The front time of the impulse is approximately proportional to the product $C_B R_D$.
3. The tail time is dependent on the product $C_S R_E$.

4.3.2 Selection of the impedance level

The capability of an impulse generator to deliver impulses depends on its impedance level. When the impedances of the generator components are high (high resistance values and low capacitance values) the energy stored in capacitors is low. In this case, a low impedance load (low resistances and high capacitances) distorts the impulse shape. This effect limits the range of resistive and capacitive loading of an impulse calibrator, as the impulse parameters should not change too much when the load is changed. Although these changes can be compensated for by parameter calculations, the impulse shape should stay within standardised limits [7].

The instruments that can be calibrated can be divided into three groups according to their impedance level: 1) high impedance inputs of measuring instruments (≥1MΩ), 2) dividers with medium input impedance (1 kΩ - 10 kΩ), and 3) low impedance digitisers, attenuators and terminators (50 Ω or 75 Ω).

Some possible loads and their typical input impedance levels are listed in Table 5.

The lower the impedance levels that the calibrator circuit should drive the lower the impedance level and higher the energy that is required from the device.

4.3.3 Influence of stray inductance

Low impedance levels are preferable if the loading capability is given the highest priority. However, the analytical calculation of a low impedance calibrator has additional sources of uncertainty. When the impedance levels are low, the currents are higher, and the stray inductances of the components and the component layout cannot be neglected. This low inductance is difficult to measure, or even estimate, accurately enough.

The self-inductance of a straight wire is approximately 1 μH/m (1 nH/mm); this value, together with an estimate of inductances of the components in the loop, gives the approximate inductance present in the circuit. Using this value, estimates for the stray inductance for low impedance and high impedance designs are 300 nH and 100 nH.

The self-resonant frequency of the impulse circuit loop formed by C_S, L_S, R_D and C_B can be calculated from

$$f_R = \frac{1}{2\pi\tau} \approx \frac{1}{2\pi\sqrt{L_S C_B}}, \tag{1}$$

The estimated stray inductance L_S of the low impedance calibrator is 300 nH and the front capacitor C_B is 10 nF. The resulting resonant frequency is approximately 3 MHz, and the corresponding time constant τ is approximately 50 ns. This is only approximately one decade faster than the front time, which means that the effect of inductance can not be neglected.

Also, this oscillation is damped only when the front resistor R_D is

$$R_D \geq \frac{4L_S}{\tau}. \tag{2}$$

For the values above, the damping resistance R_D must be larger than approximately 25 Ω. However, in order for the front time to fall within the tolerances stated in IEC 60060, between 0,84 and 1,56 μs, R_D must be between 25 and 50 Ω.

There seems to be no straightforward solution either to reduce the stray inductance to an acceptable level or make an accurate enough estimation of it, in order to get the highest accuracy required for calibration purposes.

For high impedance design with estimated stray inductance of 100 nH and front capacitor of 1 nF, the resonant frequency is approximately 16 MHz and the time constant is approximately 10 ns. The critical damping limit is achieved with R_D greater than 40 Ω. To have T_1 between 0,8 and 1,6 µs, R_D must be from 220 to 450 Ω. The resonance is not only moved to higher frequencies but is also heavily damped. The influence of stray inductance can be neglected for high impedance design.

4.3.4 Voltage range

There are several voltage level requirements (see Table 5). The input voltage levels of digitisers and peak voltmeters start from tens of millivolts ranging up to 2000 V. Component selection and availability in that voltage range is quite good.

To be able to have a meaningful output from a high voltage divider (having typically ratios from 1000 to 10000), the applied voltage should be at least some hundreds of volts.

Two designs, one for high impedance meters and the other for low impedance devices, have been adopted.

One of the designs is a high impedance calibrator optimised for accuracy. Four calibrator heads were designed using this approach, two of them produce a standard lightning impulse, with front times on the lower and higher end of the tolerance defined in IEC 60060-1. The other two produce switching impulses, one of them is defined in IEC 60060-1, and the other in 60183-1.

The low impedance design is applied only to one lightning impulse shape, for impulse calibration of high voltage dividers. A list of designed calibrator heads is in Table 6.

Table 5 Typical input impedances and practical input voltage levels of some devices that can be calibrated by impulse calibrators.

Device	R_{IN}	C_{IN}	U_{IN}
Digitiser or peak voltmeter, high impedance input	1MΩ	< 100 pF	50 mV – 1600 V
Resistive divider	1 – 20 kΩ	< 300 pF	> 1 kV
Capacitive divider	∞	< 2 nF	> 1 kV
Digitiser or peak voltmeter, low impedance input	50 or 75 Ω	-	< 10 V
Matched attenuator or terminator	50 or 75 Ω	-	< 1600 V

Table 6 List of calibrators designed and described in this thesis.

Impulse type	Design	Impulse shape	Load range	Standard(s)
Lightning	High impedance	0,84/60	< 100 pF, > 100 kΩ	IEC 60060-1, IEC 61083-1
Lightning	High impedance	1,56/60	< 100 pF, > 100 kΩ	IEC 60060-1, IEC 61083-1
Lightning	Low impedance	1,56/60	< 2 nF, > 1 kΩ	IEC 60060-1, IEC 61083-1
Switching	High impedance	250/2500	< 100 pF, > 100 kΩ	IEC 60060-1
Switching	High impedance	20/4000	< 100 pF, > 100 kΩ	IEC 61083-1

5 High impedance calibrator

5.1 Theory

This chapter describes how the impulse parameters (U_P, T_1 or T_P, and T_2) of the high impedance calibrator are calculated. The solution for calculating the peak value of an impulse circuit without inductive elements can be found in [8] or [29].

The circuit diagram showing all components of the circuit and the equivalent circuit used for analytical calculation of the impulse parameters are shown in Figure 12. For the equivalent circuit the current limiting resistor R_C, the input resistance and capacitance of the voltmeter V and the storage capacitor C_1 can be ignored because they are disconnected from the circuit when relay contact opens. Capacitor C_D, which dampens the switching surges, is shorted; and the capacitance of C_B, C_L and the connecting cable are combined and represented by C'_B.

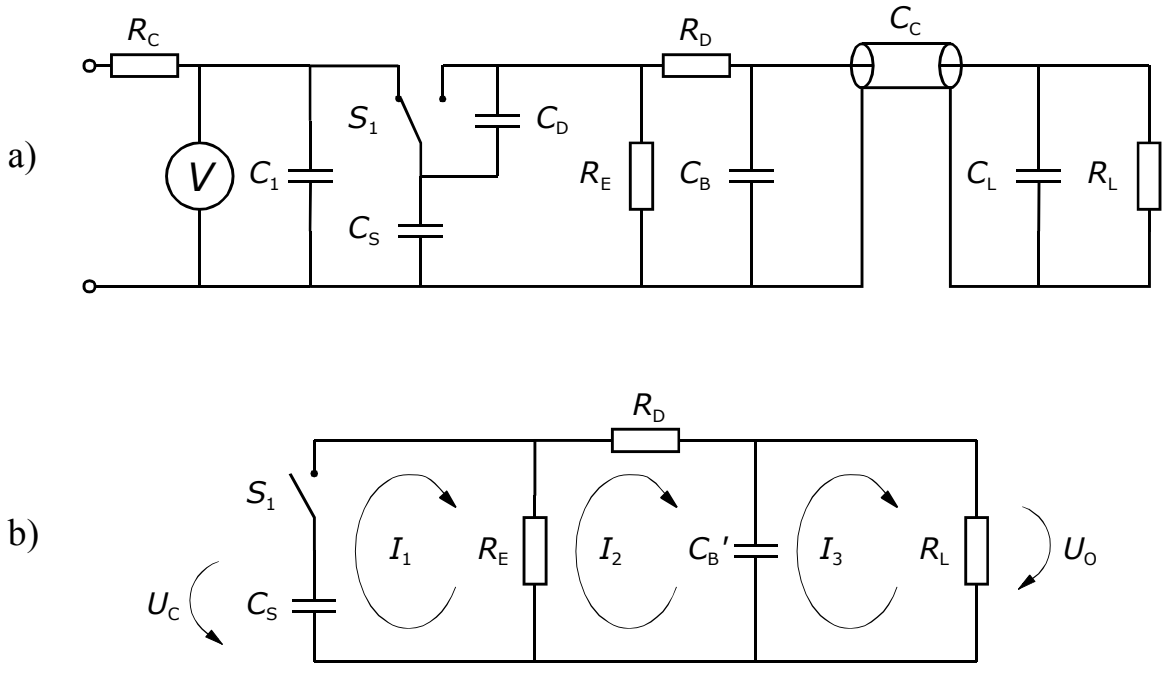

Figure 12 Relay based calibrator. a) Circuit diagram. b) Equivalent circuit for impulse parameter calculation.

The characteristics of the relay limit the maximum peak value to ±300 V. Above that voltage the relay does not show bounce free operation, and the impulses become distorted. The lower voltage limit is dictated by the charge transfer phenomenon present in the relay (see Section 5.2.2).

The solution of the circuit starts from the equivalent circuit [8, 29]. When the capacitance of the load is combined with the front capacitor of the calibrator ($C'_\mathrm{B} = C_\mathrm{B} + C_\mathrm{L}$), the matrix equation can be written using the notation shown in Figure 12b:

$$\begin{bmatrix} 1/s\,C_\mathrm{S} + R_\mathrm{E} & -R_\mathrm{E} & 0 \\ -R_\mathrm{E} & R_\mathrm{E} + R_\mathrm{D} + 1/s\,C'_\mathrm{B} & -1/s\,C'_\mathrm{B} \\ 0 & -1/s\,C'_\mathrm{B} & 1/s\,C'_\mathrm{B} + R_\mathrm{L} \end{bmatrix} \begin{bmatrix} I_1 \\ I_2 \\ I_3 \end{bmatrix} = \begin{bmatrix} U_\mathrm{C}/s \\ 0 \\ 0 \end{bmatrix}. \tag{3}$$

The solution of this matrix equation determines the branch currents:

$$\begin{bmatrix} I_1 \\ I_2 \\ I_3 \end{bmatrix} = \begin{bmatrix} R_\mathrm{E} + R_\mathrm{D} + R_\mathrm{L} + C'_\mathrm{B}\,R_\mathrm{L}(R_\mathrm{E} + R_\mathrm{D})\,s \\ R_\mathrm{E} + R_\mathrm{E}\,C'_\mathrm{B}\,R_\mathrm{L}\,s \\ R_\mathrm{E} \end{bmatrix} \cdots$$

$$\cdots \frac{U_\mathrm{C}\,C_\mathrm{S}}{R_\mathrm{E} + R_\mathrm{D} + R_\mathrm{L} + [C_\mathrm{S}\,R_\mathrm{E}(R_\mathrm{D} + R_\mathrm{L}) + C'_\mathrm{B}\,R_\mathrm{L}(R_\mathrm{E} + R_\mathrm{D})]s + C'_\mathrm{B}\,C_\mathrm{S}\,R_\mathrm{D}\,R_\mathrm{E}\,R_\mathrm{L}}. \tag{4}$$

Now, since $U_\mathrm{O} = R_\mathrm{L} I_3$, the output voltage$U_\mathrm{o}(s)$ can be determined:

$$U_\mathrm{O}(s) = U_\mathrm{C} \frac{d}{a\,s^2 + b\,s + c}, \tag{5}$$

where

$$\begin{aligned} a &= C'_\mathrm{B}\,C_\mathrm{S}\,R_\mathrm{D}\,R_\mathrm{E}\,R_\mathrm{L}, \\ b &= C_\mathrm{S}\,R_\mathrm{E}(R_\mathrm{D} + R_\mathrm{L}) + C'_\mathrm{B}\,R_\mathrm{L}(R_\mathrm{E} + R_\mathrm{D}), \\ c &= R_\mathrm{E} + R_\mathrm{D} + R_\mathrm{L} \end{aligned} \tag{6}$$

and

$$d = C_\mathrm{S}\,R_\mathrm{E}\,R_\mathrm{L}.$$

Now the circuit is solved in the frequency domain. The time domain solution can be found using the inverse Laplace transform. To be able to do that, the roots of the denominator of equation (5) must be calculated:

$$U_{\mathrm{O}}(s) = U_{\mathrm{C}} \frac{d}{a(s-g)(s-h)}, \tag{7}$$

where the sought roots, g and h, are:

$$g = \frac{-b + \sqrt{b^2 - 4ac}}{2a} \tag{8}$$

and

$$h = \frac{-b - \sqrt{b^2 - 4ac}}{2a}. \tag{9}$$

The inverse Laplace transform can now be found:

$$\boxed{u_{\mathrm{O}}(t) = U_{\mathrm{C}} \frac{d}{a(g-h)}\left(e^{gt} - e^{ht}\right)}. \tag{10}$$

This solution is a double exponential curve. For all non-oscillating waveforms, variables g and h are always real numbers and negative, which makes both exponential terms decaying.

The time to peak, t_{P}, can be solved by differentiating equation (10) and setting the derivative to zero:

$$u'_{\mathrm{O}}(t) = U_{\mathrm{C}} \frac{d}{a(g-h)}\left(g\,e^{gt} - h\,e^{ht}\right) = 0, \tag{11}$$

which yields

$$t_{\mathrm{p}} = \frac{\ln(g/h)}{h-g}. \tag{12}$$

The peak value of the impulse can now be solved by substituting this value to equation (10):

$$\hat{u}_{\mathrm{O}} = u_{\mathrm{O}}(t_{\mathrm{P}}) = U_{\mathrm{C}} \frac{d}{a(g-h)}\left(e^{g t_{\mathrm{P}}} - e^{h t_{\mathrm{P}}}\right). \tag{13}$$

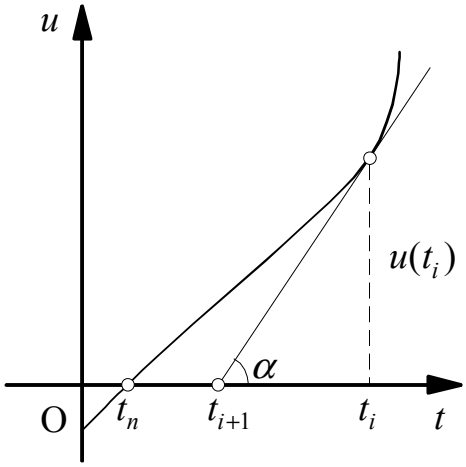

$$\tan\alpha = u'(t_\mathrm{i}) = \frac{u(t_\mathrm{i})}{t_{\mathrm{i}+1} - t_\mathrm{i}}$$

Figure 13 Graphical interpretation of Newton's iteration.

The time parameters, T_1 and T_2, cannot be solved in closed form; they must be solved by approximation. The most straightforward tool, Newton's iteration, proves to be good enough for this purpose. In Newton's iteration a new estimate for the solution is calculated from the previous estimate using

$$t_{\mathrm{i}+1} = t_\mathrm{i} - \frac{u(t_\mathrm{i})}{u'(t_\mathrm{i})}. \tag{14}$$

This has a graphical interpretation, which is shown in Figure 13. The tangent of the curve is calculated using the old estimate, t_i. This tangent is extended to the horizontal axis, and this intersection, $t_{\mathrm{i}+1}$, is used as the new estimate. The process is repeated, until the difference $t_i - t_{i+1}$ is sufficiently small.

For the evaluation of T_1 and T_2 the crossover points of the impulse front with 30% and 90% of the peak value, and the impulse tail with 50% of the peak value are needed. These are solved by setting $u_\mathrm{O}(t_{30}) = 0{,}3\,\hat{u}_\mathrm{O}$, $u_\mathrm{O}(t_{90}) = 0{,}9\,\hat{u}_\mathrm{O}$ and $u_\mathrm{O}(t_{50}) = 0{,}5\,\hat{u}_\mathrm{O}$ into the time domain solution in equation (10). This yields

$$\begin{aligned}
&U_\mathrm{C}\frac{d}{a(g-h)}\left(e^{g t_{30}} - e^{h t_{30}}\right) - 0{,}3\,\hat{u}_\mathrm{O} = 0,\\
&U_\mathrm{C}\frac{d}{a(g-h)}\left(e^{g t_{90}} - e^{h t_{90}}\right) - 0{,}9\,\hat{u}_\mathrm{O} = 0\\
&\text{and}\\
&U_\mathrm{C}\frac{d}{a(g-h)}\left(e^{g t_{50}} - e^{h t_{50}}\right) - 0{,}5\,\hat{u}_\mathrm{O} = 0.
\end{aligned} \tag{15}$$

From these t_{30}, t_{50} and t_{90} can be solved using Newton's iteration with proper initial estimates.

Now it is simple to evaluate the parameter values for the lightning impulse waveshape:

$$\begin{array}{|l|}\hline U_{\mathrm{P}} = \hat{u}_{\mathrm{O}} \\ \hline T_1 = 1{,}67\,(t_{90} - t_{30}) \\ \hline T_2 = (t_{50} - t_{30}) + 0{,}5\,(t_{90} - t_{30}) \\ \hline \end{array}, \tag{16}$$

and for the switching impulse waveshape:

$$\begin{array}{|l|}\hline U_{\mathrm{P}} = \hat{u}_{\mathrm{O}} \\ \hline T_{\mathrm{P}} = t_{\mathrm{P}} \\ \hline T_2 = t_{50} \\ \hline \end{array}. \tag{17}$$

5.2 High impedance head design

5.2.1 General

The high impedance calibrator is designed to act as a primary reference for impulse voltages. Its readings are based solely on the calculation of the impulse parameters from the known values of the components, charging voltage and the input resistance and capacitance of the device under calibration. The circuit diagram of the calibrator is shown in Figure 14 and the calibrator itself in Figure 15. All components in the impulse circuit are passive.

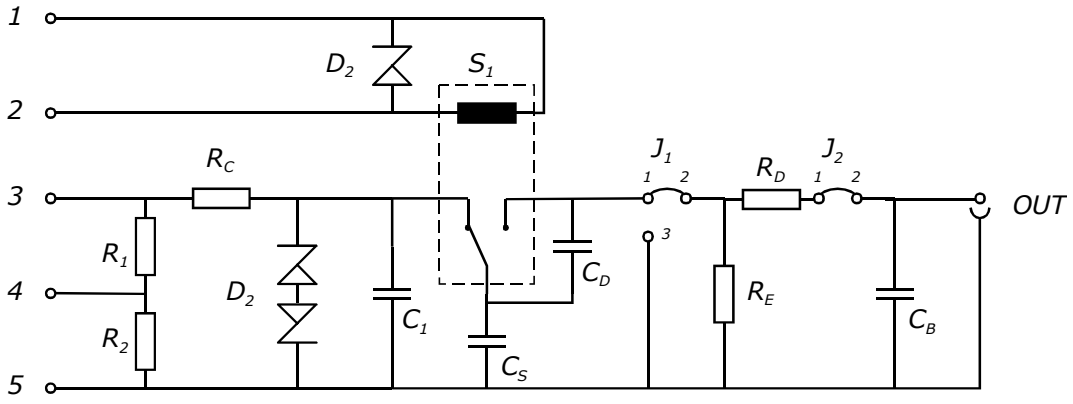

Figure 14 Schematic diagram of the relay based calibrator.

A charging voltage is supplied between terminals 3 and 5. When relay S_1 is not energised (shown in that position in the Figure), capacitor C_S is charged. The charging voltage is measured by a digital multimeter. After the charging voltage is measured, the relay is activated to disconnect C_S from the charging source and connect it to the pulse-shaping network.

Resistors R_1 and R_2 are used for the recognition of the calibrator head. During the charging phase the voltage between terminal 4 and 5 is measured, too, to detect the ratio of the divider formed by R_1 and R_2. The ratio of this divider is different for each constructed calibrator.

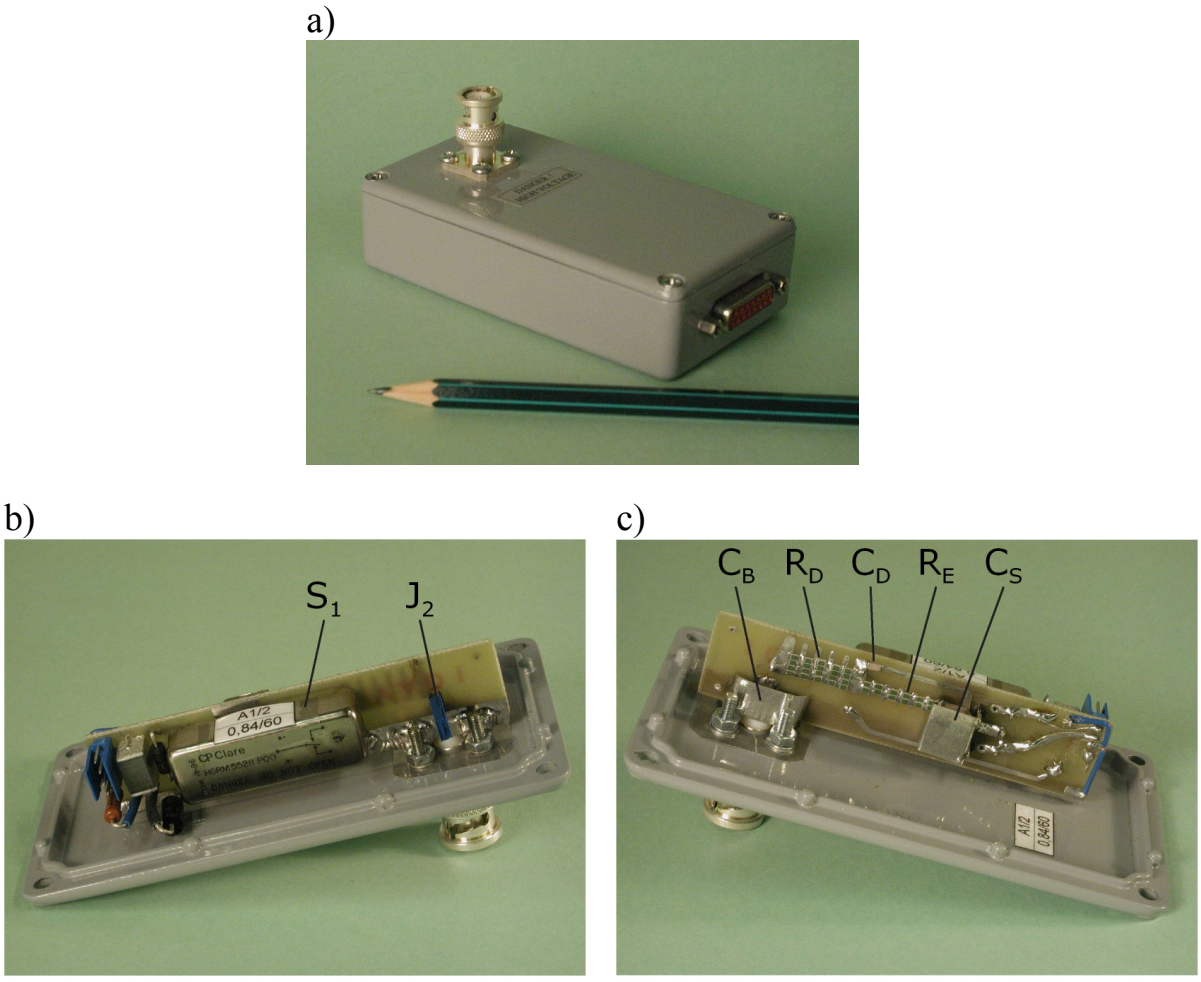

Figure 15 High impedance calibrator head prototype.
a) Outside view
b) Downside of the printed circuit board
c) Upside of the printed circuit board.

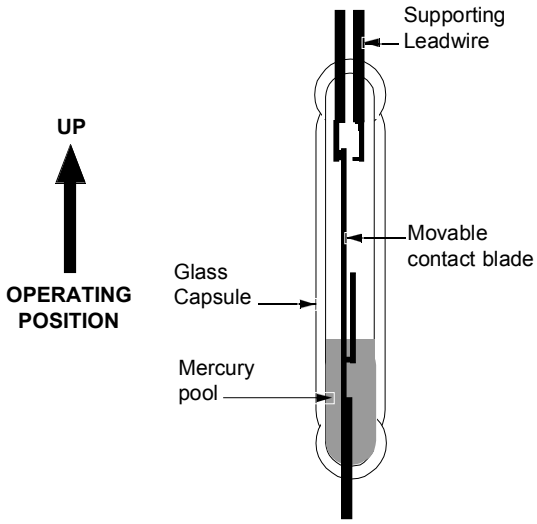

Figure 16 Mercury-wetted relay [30]. The activation coil is not shown.

Capacitance C_1 is added for reducing the charge transfer effect and C_D for damping the switching transients. C_1 is disconnected from the circuit and C_D shorted when the relay is activated, and they can so be ignored from the calculation. For more detailed explanation see Section 5.2.2.

Resistor R_C limits the charging current and Zener diodes Z_1 and Z_2 protect the circuit from overload.

5.2.2 Mercury-wetted relay

Regardless of the recent advances in semiconductor switching technology, the most ideal switching element remains a mechanical reed relay with mercury wetted contacts. The structure of a mercury-wetted relay is shown in Figure 16. It has a small amount of mercury in a high-pressure hydrogen environment. A drop of mercury is pulled by capillary force onto the contact surface. This prevents arcing, and thus the relay makes a bounce-free contact in less than 1 ns. The relay is activated by a magnetic field that can be introduced by a magnet or a coil around the glass capsule.

The switch itself works, for this application, as an ideal switch. However, the coil around it causes a degree of difficulty because of the capacitive coupling between the contacts and the coil. This produces an effect known as “charge transfer”, whereby a charge is transferred from the change of the energising voltage to the contacts of the relay through the capacitance between them.

Adding a shield between the reed tube and the energising coil reduces this effect by allowing the magnetic field to activate the contacts while shielding the contact from capacitive interference from the coil.

Without a capacitive shield the capacitance between an open contact and coil is approximately 10 pF. When the coil energised, the potential of its other end is raised to 10 V. This voltage step introduces a charge $\Delta Q = C\,\Delta U \approx 10\,\text{pF} \cdot 10\,\text{V} = 0{,}1\,\text{nC}$ into the contact through the coil-contact capacitance. This charge is injected into capacitor C_S, which sees a voltage change $\Delta U = \Delta Q / C_S$. The value of C_S is approximately 20 nF for lightning impulse and 50 nF for switching impulse; so the maximum voltage change introduced into the charging capacitor is $0{,}1\,\text{nC} \,/\, 20\,\text{nF} = 0{,}5\,\text{mV}$. For charging voltages below 0,5 V, this represents more than 0,1% of the peak value, and the effect should be taken into account.

In this case adding a large capacitor (C_1) in parallel with the critical capacitor, (C_S) reduces the effects of charge transfer. When the coil is energised, the transferred charge is distributed to both of these capacitors. C_1 is larger in value, and thus takes most of the transferred charge. The effect on the charging voltage is in this case reduced by a factor of approximately 10. The charge transfer effect can be ignored for charging voltages above 50 mV.

An extensive search was conducted in order to find a relay with as high an operating voltage as possible. A bounce free switching voltage of 300 V was achieved using relays with nominal switching voltage of 500 V (CP Clare Corporation, type HGRM), when a damping capacitor (C_D) was used between the closing contacts.

5.2.3 Capacitors

The principal requirements for impulse forming network capacitors were stability and low losses. This directly pointed to NPO type ceramic capacitors, which have very small temperature coefficient. The typical specification is ±30 ppm/K. The additional requirements, medium range capacitance values and voltage withstand of 500 V, narrowed the selection to a small number of multilayer types, and the final decision among the candidates was dictated by their availability in small quantities. The major characteristics of the chosen capacitor are shown in Table 7.

Table 7 Principal specifications of the capacitors used in the high impedance calibrator.

Type	Multilayer ceramic
Capacitance values	330 pF / 4,7 pF
Dielectric	NPO
Temperature coefficient	± 30 ppm/K
Tolerance	± 10%
Dissipation factor	$\leq 25 \times 10^{-3}$ @ 1 kHz
Rated voltage	500 V
Proof voltage	850 V, 5 s

Two different capacitance values from the same manufacturer were selected for the calibrator. Their voltage dependence was measured by comparison with an air-insulated reference capacitor. This reference capacitor was known to have a negligible temperature and voltage coefficient. The tested capacitors showed low voltage coefficient, the change of capacitance in the operating voltage range was less than 0,05%. The average results derived from the measurements of three samples are shown in Figure 17.

Similarly, the stability of the capacitors was verified. Calibration results of one of the impulse heads over a period of approximately 2 years are shown in Figure 18. It has been in extensive use in a worldwide intercomparison project [31]. Again, the components were found to be stable; the difference between the highest and lowest measured value was less than 0,15%, which is at the limit of the estimated uncertainty of the calibration.

As capacitors with sufficiently high capacitance were not easily available, several components were connected in parallel. The components used for each of the capacitor stacks are summarised in Table 8.

5.2.3.1 Capacitor calibration

The links J1 and J2 (see Figure 14) were added into the circuit to enable calibration of the capacitors. For calibration of C_B link J_2 is opened. Capacitance

of C_B can now be measured from the output BNC connector, without having resistors R_E and R_D in parallel. Two wire capacitance measurement techniques can be used, which means that only the capacitance of the measuring cable is measured first, and this reading is subtracted from the sum capacitance of the cable and C_B.

To measure the capacitance of C_S, link J_1 is opened and the relay driven in closed position (C_D is now shorted). The capacitance of C_S is measured between terminals 1 and 3 of J_1, using a subtraction method similar to that described for C_B measurement.

Table 8 The nominal values of the tail and front capacitors.

Impulse shape	C_S	C_B
0,84/60	18,8 nF (4 * 4,7 nF)	1,32 nF (4 * 0,33 nF)
1,56/60	18,8 nF (4 * 4,7 nF)	1,32 nF (4 * 0,33 nF)
20/4000	56,4 nF (12 * 4,7 nF)	9,4 nF (2 * 4,7 nF)
250/2500	56,4 nF (12 * 4,7 nF)	9,4 nF (2 * 4,7 nF)

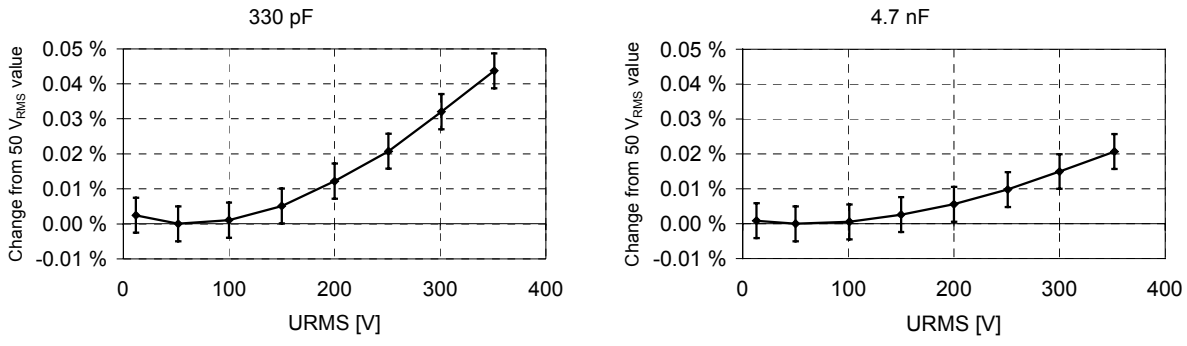

Figure 17 Measured voltage dependence of capacitance of both types of capacitors used in the high impedance calibrator.

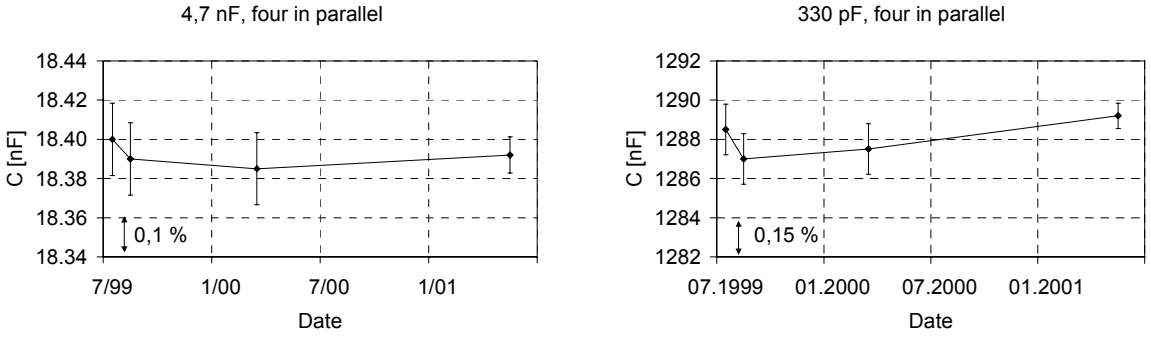

Figure 18 The stability of the capacitors used in the high impedance calibrator. The samples show the calibration results of a parallel connection of four 4,7 nF capacitors used as C_S (left) and four 330 pF capacitors used as C_B (right). The error bars show the estimated uncertainty of each calibration (k=2).

Table 9 Principal specifications of the individual resistors used in the high impedance calibrator.

Type	Thin film SMD
Resistance values	From 174 Ω to 16,9 kΩ
Temperature coefficient	± 10 ppm/K
Tolerance	± 0,1%
Max. working voltage	100 V
Max. overload voltage	200 V
Rated power	0,1 W

5.2.4 Resistors

The resistors for this circuit should have a low temperature coefficient and high bandwidth. These requirements were strictly followed and thin film surface mount device (SMD) type resistors were selected. Because the resistors with the lowest temperature coefficient were not readily available for 500 V, several resistors were connected in series. An overview of the specifications of the selected resistors is in Table 9. The results of intermittent calibrations are shown in Figure 19.

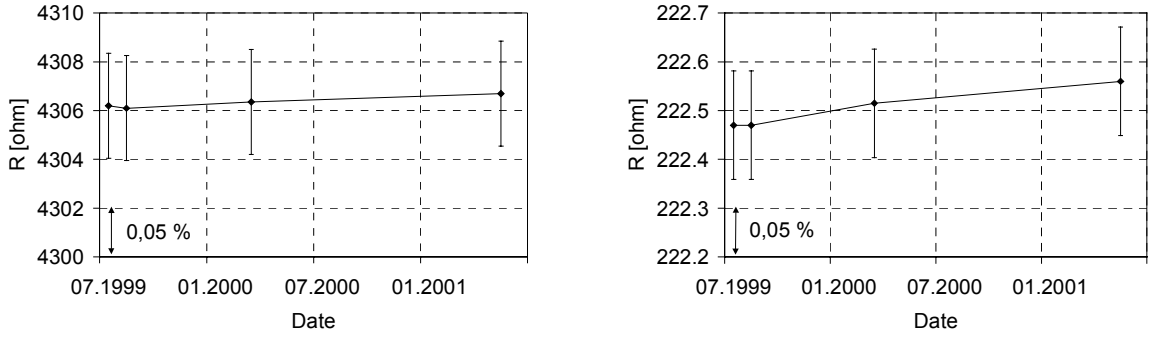

Figure 19 The stability of the resistors used in the high impedance calibrator. The samples show the calibration results of R_E (left) and R_D (right). Both are built by connecting several resistors in series and parallel. The error bars show the estimated uncertainty of each calibration (k=2).

Table 10 The nominal values of the tail and front resistors. Each resistor is made of five components in series and 1 – 4 in parallel.

Impulse shape	R_E	*Parallel components*	*Component values*
0,84/60	222,5 Ω	4	174 Ω, 182 Ω
1,56/60	448,3 Ω	4	309 Ω, 357 Ω, 422 Ω
20/4000	331 Ω	2	121 Ω, 140 Ω
250/2500	7,95 kΩ	2	2,94 kΩ, 3,24 kΩ
Impulse shape	R_D	*Parallel components*	*Component values*
0,84/60	4306 Ω	2	1,37 kΩ, 1,50 kΩ
1,56/60	4206 Ω	2	1,37 kΩ, 1,50 kΩ
20/4000	97,6 kΩ	1	15,0 kΩ, 16,9 kΩ
250/2500	52,43 kΩ	1	8,06 kΩ, 8,87 kΩ

The voltage and energy withstand characteristics of single resistors are again not enough for their intended task. Five resistors are used in series to reach the voltage withstand requirement, and from 1 to 4 in parallel to reduce the energy absorption requirement of individual resistors. The build-up of the front and tail resistors from single components is shown in Table 10. The capacitance values

were measured first, and the resistance values were adjusted to obtain the nominal impulse shape into 1 MΩ, 35 pF load.

Measurements at 100 kHz indicate that the inductance is less than 100 nH for all R_E resistors. The inductance is higher for the lower resistor values, and for the 7,95 kΩ resistor a small parallel capacitance (<1 pF) was measured instead of series inductance.

5.2.5 Circuit board layout

The components are soldered onto a small printed circuit board (PCB). It was designed to be compact, so that the stray inductances were as low as possible.

The calibration of the components was additionally taken into account in the PCB design. The values of the resistors and capacitors can be measured without removing them from the circuit board. Small shields are mounted around the capacitors; they shield the capacitors from changes in stray capacitances when the box is open for capacitor calibration.

The PCB is mounted in an asymmetrical box. The connectors are mounted so, that the box will hang downwards from the connector of the DUC, and the relay will be correctly oriented (see Figure 9).

5.3 Uncertainty analysis

Before a justified uncertainty analysis can be made, the traceability of related measurements has to be clarified. For the high impedance calibrator this means that both the measurements of the components of the generator circuit and the charging voltage measurement have to be considered. A detailed traceability chain for a lightning impulse calibrator is shown in Figure 20.

The uncertainty estimates have been built following the guidelines set by a guide published by the European co-operation for Accreditation (EA), "*Expression of the Uncertainty of Measurement in Calibration*" [32]. A commercial software package [33], based on the method described in the guide, is used for creating the uncertainty budget tables.

An overview of the basic terms and techniques of uncertainty estimation is presented in Appendix A.

The contribution of the following sources of uncertainty are considered in the uncertainty analysis:

- Calculation, verification of the formulas
- Capacitors, calibration uncertainty
- Capacitors, temperature coefficient
- Capacitors, voltage coefficient
- Resistors, calibration uncertainty
- Resistors, temperature coefficient
- Relay, charge transfer
- Load resistance, measurement uncertainty
- Load capacitance, measurement uncertainty
- Charging voltage measurement uncertainty
- Stray inductance

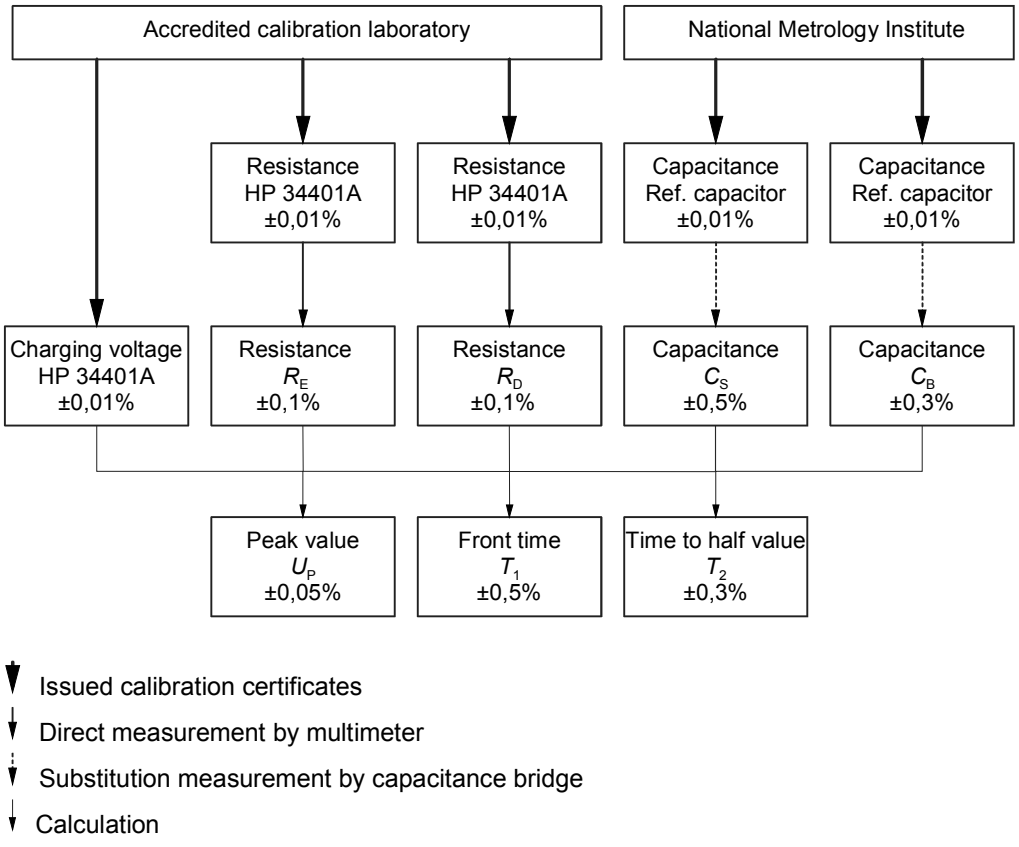

Figure 20 Traceability chain of the high impedance calibrator. Order of magnitude of the uncertainties (k=2) in each stage is shown for lightning impulse heads.

5.3.1 Sensitivity of the calculation

A sensitivity analysis was done for the formulae used for parameter calculation. This analysis revealed that the calculated impulse peak value was not sensitive to variations in any one of the component values in formula 13 for evaluating U_P. The sensitivity analysis was carried out by differing the value of each input parameter of the formula by 1%, and observing the resulting changes in calculated parameter values. As shown in Table 11 and Table 12, only the uncertainty in the charging voltage is directly reflected in the peak value accuracy; small change in any component has minimal influence on this. For a 0,1% change in the peak value, for example, any single component of the impulse circuit must change by more than 1%. Only the charging voltage must be measured with the same level of uncertainty that required for the calibrator impulses.

For the time parameters the situation is not as favourable as for the peak value. The front time is sensitive to changes in the values of the front resistor and capacitor (R_D and C_B), and the time to half value to changes in the tail resistor and capacitor (R_E and C_S). In both cases, the changes are directly related to the corresponding time parameter, for example a 1% increase in R_D causes a 1% change to the front time.

5.3.2 Uncertainty of capacitor calibration

Care was exercised in the calibration of the impulse circuit capacitors. The capacitance of the measuring leads was minimised, and compensated for (see section 5.2.3.1). The measured average values of the capacitors together with statistical information are presented in Table 13. A pooled estimate for the uncertainty of each capacitance calibration is used. This estimate takes into account the uncertainty of the capacitance of the reference capacitor and that of the substitution method used for the capacitance calibration.

The voltage dependence was also checked, and the capacitance increases approximately 0,05% from 0 to 300 volts. This is included in the uncertainty budget as a rectangular distribution, with a lower limit of 0,00% and an upper limit of 0,05%.

The temperature dependence was not measured, but its influence was estimated based on the specifications. A range of operating temperature was set to be (22 ± 10) ºC, the specified voltage coefficient (between ± 0,0003%/K) was

multiplied by five, and a rectangular distribution from –0,0015% to +0,0015% was used for uncertainty estimation.

The voltage and temperature effects have a minimal influence on the capacitance uncertainty; the major factor is the uncertainty in the capacitance value calibration.

To have an ample margin for the uncertainty budget, conservative uncertainty estimates of 0,3% for C_B and 0,5% for C_S are used for the uncertainty budgets. These estimates include both temperature and voltage dependent changes in the capacitors.

Table 11 Sensitivity of the parameter calculation to uncertainties in the input quantities for lightning impulse, a) 0,84/60, b) 1,56/60.

a)

LI 0,84/60		Sensitivity [%/%]		
Component	Nominal value	U_P	T_1	T_2
C_S	18,8 nF	0,08	0,10	0,91
C_B	1,32 nF	-0,08	0,87	0,09
R_E	4306 Ω	0,02	0,04	0,97
R_D	222,5 Ω	-0,02	0,96	0,03
R_L	1 MΩ	0,0003	0,0004	0,004
C_L	40 pF	-0,002	0,03	0,003
U_C	100 V	1,00		

b)

LI 1,56/60		Sensitivity [%/%]		
Component	Nominal value	U_P	T_1	T_2
C_S	18,8 nF	0,09	0,13	0,89
C_B	1,32 nF	-0,09	0,84	0,11
R_E	4206 Ω	0,03	0,07	0,94
R_D	448,3 Ω	-0,03	0,93	0,05
R_L	1 MΩ	0,0005	0,0007	0,004
C_L	40 pF	-0,003	0,03	0,003
U_C	100 V	1,00		

Table 12 Sensitivity of the parameter calculation to uncertainties in the input quantities for switching impulse, a) 20/4000, b) 250/2500.

a)

SI 20/4000		Sensitivity [%/%]		
Component	Nominal value	U_P	T_1	T_2
C_S	56,4 nF	0,14	0,23	0,85
C_B	9,4 nF	-0,15	0,76	0,15
R_E	97,6 kΩ	0,003	0,12	0,91
R_D	331 Ω	-0,003	0,87	0,005
R_L	1 MΩ	0,0005	0,012	0,09
C_L	40 pF	-0,0006	0,003	0,0006
U_C	100 V	1,00		

b)

SI 250/2500		Sensitivity [%/%]		
Component	Nominal value	U_P	T_1	T_2
C_S	56,4 nF	0,19	0,31	0,78
C_B	9,4 nF	-0,19	0,69	0,22
R_E	52,43 kΩ	0,06	0,22	0,85
R_D	7,95 kΩ	-0,07	0,76	0,10
R_L	1 MΩ	0,008	0,02	0,05
C_L	40 pF	-0,0002	0,0007	0,0002
U_C	100 V	1,00		

Table 13 Calibration results of high impedance calibrator capacitors.

N=4	Average value	Estimated uncertainty of each observation (k=2)	Standard deviation of the observations
C_S	18,392 nF	0,1%	0,03%
C_B	1,2881 nF	0,2%	0,08%

5.3.3 Uncertainty of resistor calibration

Each resistance measurement was conducted using four-wire measuring technique. In this way, the resistance of the measuring cables does not affect the results significantly. Again, a pooled estimate was used for the uncertainty; the calibration uncertainty of the meter was 0,005% on the ranges used, ten times that was estimated as the uncertainty of each observation of the resistances. The average value, the pooled estimate and the standard deviation of the results are shown in Table 14.

Again, a conservative value of 0,1% is used for the calibrated resistance values in the uncertainty budget. This includes temperature dependent changes in the resistors.

5.3.4 Relay charge transfer

The amount of charge transferred from the coil to the contacts depends on the voltage step applied to the coil and the effective stray capacitance between the coil and the contacts. As the transferred charge is not dependent on the charging voltage, its influence is significant only when the charging voltage is low.

The effect of charge transfer is according to the estimation presented in section 5.2.2 approximately 0,05 mV on the peak value. For 50-mV impulses this is 0,1% of the peak value. The effect also appeared in measurements as a polarity effect. For voltages above 500 mV the effect is less than 0,01% of the peak values, and it can be ignored.

5.3.5 Impedance of the load

For the calculation to yield correct results the input impedance of the device under calibration must not change significantly with voltage, and it should be possible to model it using a resistance R_L in parallel with a capacitance C_L (see Figure 12a).

Table 14 Calibration results of high impedance calibrator resistors.

N=4	Average value	Estimated uncertainty of each observation (k=2)	Standard deviation of the observations
R_E	4306,3 Ω	0,05%	0,01%
R_D	222,50 Ω	0,05%	0,02%

For example the Zener diode based system proposed by Kiseliev [28] does not fulfil this requirement. This measuring device has a high input resistance up to the Zener voltage. When that is exceeded the Zener diodes start to conduct, and the meter input impedance changes abruptly to a very low value. This behaviour can not be modelled by a simple parallel connection of a resistor and capacitor.

A typical digitiser has an input resistance R_L of approximately 1 MΩ and input capacitance C_L of approximately 30 – 50 pF. These values can be measured using an inexpensive and simple handheld multimeter, and the estimated uncertainties of these measurements are 1% for the resistance and 4 pF for the capacitance. The accuracy is low but adequate, as the parameter calculation is not very sensitive to changes in R_L and C_L.

5.3.6 Uncertainty of charging voltage measurement

The charging voltage is measured using a calibrated multimeter. Its 1-year specification for direct voltage measuring uncertainty in the range from 50 mV to 1000 V is better than 0,003% (k=2). Again, taking into account the wiring from the calibrator head to the multimeter, a conservative value of 0,02% is used for the uncertainty budget.

5.3.7 Stray inductance

A conservative estimate for the stray inductance of the loop formed by C_S, the relay, R_D and C_B is 100 nH. The effect of addition of this inductance into the formulae is 0,001% for peak value, -0,04% for the front time, and -0,002% for time to half value. The effect of this inductance is neglected.

5.3.8 Uncertainty budget

The uncertainty budgets can be made for each calibrator's parameters using the sensitivity coefficients and the uncertainty estimates presented in the previous sections. The uncertainty budgets for lightning impulse calibrator heads are shown in Tables 15 and 16. Similar budgets for switching impulse calibrator heads are presented in Tables 17 and 18. A more detailed presentation of an uncertainty budget for the peak value of a high impedance head for 0,84/60 impulse shape is presented in Appendix B.

Table 15 Uncertainty budget for LI impulse 0,84/60

LI 0,84/60			**Uncertainty budget for peak value (U_P)**		**Uncertainty budget for front time (T_1)**		**Uncertainty budget for time to half value (T_2)**	
Quantity (Component)	Nominal value	Uncert. (k=2)	Sensitivity	Contrib. to uncert.	Sensitivity	Contrib. to uncert.	Sensitivity	Contrib. to uncert.
		%	% / %	%	% / %	%	% / %	%
Capacitance (C_S)	18,8 nF	0,3	0,08	0,024	0,10	0,031	0,91	0,272
Capacitance (C_B)	1,32 nF	0,5	-0,08	0,039	0,87	0,433	0,09	0,045
Resistance (R_E)	4306 Ω	0,1	0,02	0,002	0,04	0,004	0,97	0,097
Resistance (R_D)	225,5 Ω	0,1	-0,02	0,002	0,96	0,096	0,03	0,003
Capacitance (C_L)	40 pF	10	0,0003	0,003	0,0004	0,0004	0,004	0,004
Resistance (R_L)	1 MΩ	5	-0,002	0,012	0,027	0,135	0,003	0,014
Voltage (U_C)	100 V	0,02	1,00	0,02				
Overall uncertainty (k=2)				**0,05**		**0,46**		**0,29**

Table 16 Uncertainty budget for LI impulse 1,56/60

LI 1,56/60			**Uncertainty budget for peak value (U_P)**		**Uncertainty budget for front time (T_1)**		**Uncertainty budget for time to half value (T_2)**	
Quantity (Component)	Nominal value	Uncert. (k=2)	Sensitivity	Contrib. to uncert.	Sensitivity	Contrib. to uncert.	Sensitivity	Contrib. to uncert.
		%	% / %	%	% / %	%	% / %	%
Capacitance (C_S)	18,8 nF	0,3	0,09	0,027	0,13	0,038	0,89	0,266
Capacitance (C_B)	1,32 nF	0,5	-0,09	0,044	0,84	0,422	0,11	0,054
Resistance (R_E)	4206 Ω	0,1	0,03	0,003	0,07	0,007	0,94	0,094
Resistance (R_D)	448,3 Ω	0,1	-0,03	0,003	0,93	0,093	0,05	0,005
Capacitance (C_L)	40 pF	10	0,0005	0,005	0,0007	0,0007	0,004	0,004
Resistance (R_L)	1 MΩ	5	-0,003	0,014	0,026	0,131	0,003	0,017
Voltage (U_C)	100 V	0,02	1,00	0,02				
Overall uncertainty (k=2)				**0,06**		**0,45**		**0,29**

Table 17 Uncertainty budget for SI impulse 20/4000.

SI 20/4000			**Uncertainty budget for peak value (U_P)**		**Uncertainty budget for front time (T_P)**		**Uncertainty budget for time to half value (T_2)**	
Quantity (Component)	Nominal value	Uncert. (k=2)	Sensitivity	Contrib. to uncert.	Sensitivity	Contrib. to uncert.	Sensitivity	Contrib. to uncert.
		%	% / %	%	% / %	%	% / %	%
Capacitance (C_S)	56,4 nF	0,3	0,14	0,043	0,23	0,070	0,85	0,256
Capacitance (C_B)	9,4 nF	0,5	-0,15	0,073	0,76	0,380	0,15	0,073
Resistance (R_E)	97,6 kΩ	0,1	0,00	0,000	0,12	0,012	0,91	0,091
Resistance (R_D)	331 Ω	0,1	0,00	0,000	0,87	0,087	0,01	0,001
Capacitance (C_L)	40 pF	10	0,0005	0,005	0,0116	0,0116	0,088	0,088
Resistance (R_L)	1 MΩ	5	-0,001	0,003	0,003	0,017	0,001	0,003
Voltage (U_C)	100 V	0,02	1,00	0,02				
Overall uncertainty (k=2)				**0,09**		**0,40**		**0,29**

Table 18 Uncertainty budget for SI impulse 250/2500.

SI 250/2500			**Uncertainty budget for peak value (U_P)**		**Uncertainty budget for front time (T_P)**		**Uncertainty budget for time to half value (T_2)**	
Quantity (Component)	Nominal value	Uncert. (k=2)	Sensitivity	Contrib. to uncert.	Sensitivity	Contrib. to uncert.	Sensitivity	Contrib. to uncert.
		%	% / %	%	% / %	%	% / %	%
Capacitance (C_S)	56,4 nF	0,3	0,19	0,056	0,31	0,093	0,78	0,235
Capacitance (C_B)	9,4 nF	0,5	-0,19	0,094	0,69	0,343	0,22	0,109
Resistance (R_E)	54,4 kΩ	0,1	0,06	0,006	0,22	0,022	0,85	0,085
Resistance (R_D)	7,95 kΩ	0,1	-0,07	0,007	0,76	0,076	0,10	0,010
Capacitance (C_L)	40 pF	10	0,008	0,08	0,016	0,016	0,05	0,046
Resistance (R_L)	1 MΩ	5	-0,0002	0,001	0,001	0,004	0,000	0,001
Voltage (U_C)	100 V	0,02	1,00	0,02				
Overall uncertainty (k=2)				**0,14**		**0,36**		**0,28**

6 Low impedance calibrator

6.2 Theory

This chapter describes how the impulse parameters (U_P, T_1 or T_d, and T_2) of the low impedance calibrator are calculated. Publications [20-23] from the 1950's and 1960's are used as a starting point for the solution of the case including one inductive element.

The circuit diagram and the equivalent circuit differ slightly from that used for the relay-based realisation. The FET selected makes it possible to use voltages of up to 2000 V. However, the current solution has been designed to produce impulses with peak voltages of up to 1000 V. This calibrator has also been designed for using lower impedance components, and the inductance of the circuit cannot be ignored. The addition of one more energy-storing element renders the solution slightly more complicated.

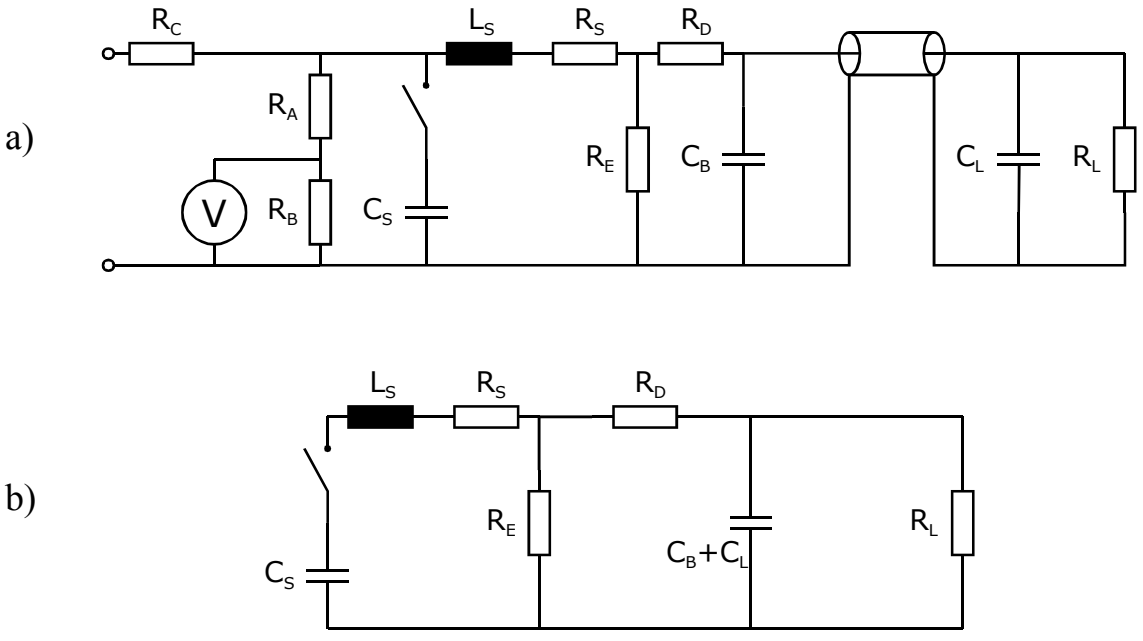

Figure 21 FET switch based calibrator. a) Circuit diagram. b) Equivalent circuit for impulse parameter calculation.

Again, the capacitance of the load and the front capacitor of the calibrator are combined ($C'_B = C_B + C_L$). Now, using the notation shown in Figure 21b, the matrix equation is:

$$\begin{bmatrix} 1/sC_S + sL_S + R_S + R_E & -R_E & 0 \\ -R_E & R_E + R_D + 1/sC'_B & -1/sC'_B \\ 0 & -1/sC'_B & 1/sC'_B + R_L \end{bmatrix} \begin{bmatrix} I_1 \\ I_2 \\ I_3 \end{bmatrix} = \begin{bmatrix} U_C/s \\ 0 \\ 0 \end{bmatrix}. \quad (18)$$

Now, since $U_O = R_L I_3$, the output voltage can be determined. The frequency domain solution now contains a third order polynomial in the numerator:

$$U_O(s) = U_C \frac{d}{s^3 + a\,s^2 + b\,s + c}, \quad (19)$$

where

$$a = \frac{R_L\,C'_B[R_D\,R_S + R_E(R_D + R_S)] + L_S(R_E + R_D + R_L)}{R_L\,L_S\,C'_B(R_E + R_D)},$$

$$b = \frac{R_L\,C'_B(R_D + R_E) + C_S[R_S(R_D + R_L) + R_E(R_D + R_S + R_L)]}{R_L\,L_S\,C_S\,C'_B(R_E + R_D)},$$

$$c = \frac{R_E + R_D + R_L}{R_E\,R_L\,L_S\,C_S\,C'_B + R_D\,R_L\,L_S\,C_S\,C'_B} \quad (20)$$

and

$$d = \frac{C_S\,R_E\,R_L}{R_E\,R_L\,L_S\,C_S\,C'_B + R_D\,R_L\,L_S\,C_S\,C'_B}.$$

A trigonometric solution for the roots of the third order polynomial in the denominator of equation (19) can be used. For the non-oscillatory case the solution can be found without the use of complex arithmetic by using the trigonometric solution of a third degree polynomial. By using substitution $s = z - a/3$, the third order equation can be rewritten as

$$z^3 + p\,z + q = 0. \quad (21)$$

where

$$p = b - \frac{1}{3}a^2,$$

$$q = \frac{2}{27}a^3 - \frac{1}{3}ab + c \tag{22}$$

and

$$D = \left(\frac{p}{3}\right)^3 + \left(\frac{q}{2}\right)^2.$$

In the non-oscillatory case ($D < 0$) the roots can be found by using the following formulae:

$$\begin{aligned}
\varphi &= \arccos\left(\frac{3q}{2p}\sqrt{\frac{3}{-p}}\right),\\
z_1 &= 2\sqrt{-\frac{p}{3}}\cos\frac{\varphi}{3},\\
z_2 &= -2\sqrt{-\frac{p}{3}}\cos\left(60^\circ + \frac{\varphi}{3}\right),\\
z_3 &= -2\sqrt{-\frac{p}{3}}\cos\left(60^\circ - \frac{\varphi}{3}\right)
\end{aligned} \tag{23}$$

and

$$s_n = z_n - \frac{1}{3}a.$$

Now, equation (19) can be rewritten in a form

$$U_O(s) = U_C\frac{d}{(s-s_1)(s-s_2)(s-s_3)}, \tag{24}$$

for which the inverse Laplace transform can be found:

$$\begin{aligned}
&u_O(t) =\\
&= U_C\, d\left(\frac{e^{s_1 t}}{(s_1-s_2)(s_1-s_3)} - \frac{e^{s_2 t}}{(s_1-s_2)(s_2-s_3)} - \frac{e^{s_3 t}}{(s_1-s_3)(s_3-s_2)}\right)
\end{aligned} \tag{25}$$

This solution is a triple exponential curve. For all non-oscillating impulses terms s_1, s_2, and s_3 are always negative, which makes the three exponential terms decaying.

In this case, the time to peak cannot be solved in a closed form. Newton's iteration is again used to find the solution. At the peak the derivative of the impulse is zero:

$$u_{\mathrm{o}}'(t) = 0\,, \tag{26}$$

Newton's iteration of equation (14) can now be used to find the solution for the zero crossing of the first derivative:

$$t_{\mathrm{i+1}} = t_{\mathrm{i}} - \frac{u'(t_{\mathrm{i}})}{u''(t_{\mathrm{i}})}\,. \tag{27}$$

This iteration will result in the time to peak, t_{P}, and subsequently, the principle for the solution of the other parameters is the same as that used with the relay based calibrator (starting from equation (13)).

6.3 Low impedance calibrator design

The low impedance calibrator additionally can deliver impulses to low impedance devices, such as resistive and capacitive dividers. Furthermore, higher voltages can be reached when the mercury wetted relay is replaced with a solid state switch.

However, the component-based calibration of this calibrator does not produce as accurate results as for the high impedance calibrator because of the higher stray inductance of the pulse-forming network. On the one hand, the components are larger because of the higher voltage rating, and the size increases the inductance. On the other hand, the loop formed by C_{S}, L_{S}, R_{D} and C_{B} is also larger. Although all effort was made to choose low inductance components and minimise the size of the inductive loop, the remaining stray inductance, some hundreds of nanohenries, can not be neglected.

With the low voltage design the accuracy of U_{P} and T_2 is comparable with that of the high impedance design. However, the accuracy of T_1 is limited by the uncertainty of the estimation of the stray inductance of the circuit. In fact, no reliable way to measure the stray inductance was found, and the inductance parameter is adjusted by comparison so that the T_1 value matches with the high impedance calibrator reading.

The circuit diagram of the calibrator impulse network is shown Figure 22. This design uses a FET switch module for impulse generation, which enables higher

charging voltages and larger currents than the values used with the mercury wetted relay. This switch (S_1) is not a changeover type, so an additional relay (S_2) is used to disconnect the impulse circuit from the charging voltage. This relay has two pairs of contacts; one is used to disconnect the charging voltage, and the second to synchronise the triggering of the FET. The charging voltage is supplied between terminals 3 and 5.

Figure 22 shows the switches in charging position. A voltage divider (formed by R_A and R_B) is used to attenuate the voltage by a factor of approximately 100. The attenuated voltage is measured using a digital voltmeter. When a trigger signal is supplied between terminals 1 and 2, relay S_2 disconnects the impulse circuit from the charging supply. Another pair of contacts gives a command to the FET module to trigger the impulse.

The second pair of contacts of relay S_2 is used for the timing of switch S_1. A small current flows through switch S_1 when it is in the offstate, and the time between disconnection of the charging voltage and impulse generation should be short enough to not discharge C_S. With this arrangement the impulse is triggered within tens of microseconds after the charging voltage has been disconnected, and discharging of C_S through S_1 can be neglected.

The components are soldered onto two printed circuit boards (see Figure 23c). One has the components of the impulse circuit; the other is for the components for charging current limitation, charging voltage measurement, protecting the relay, and synchronising the FET trigger with relay opening.

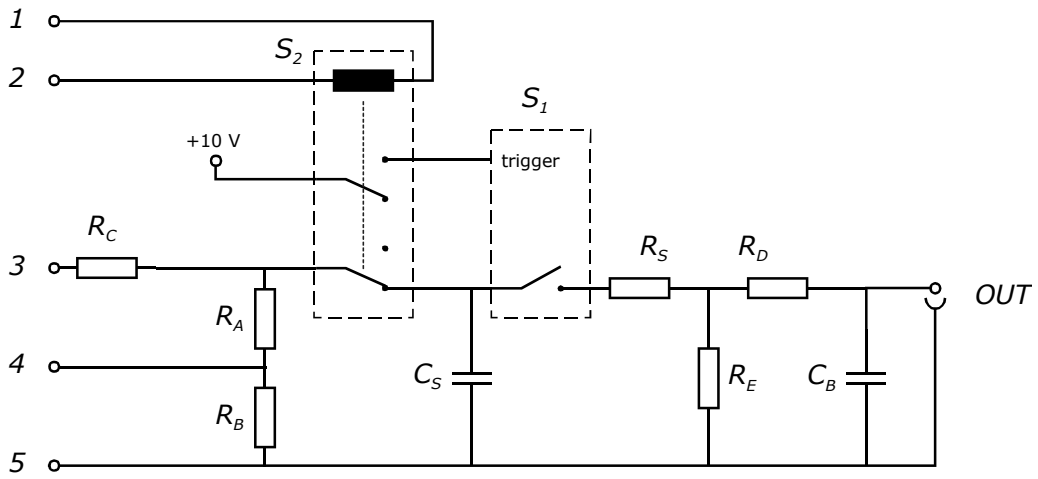

Figure 22 Simplified schematic diagram of the FET based calibrator.

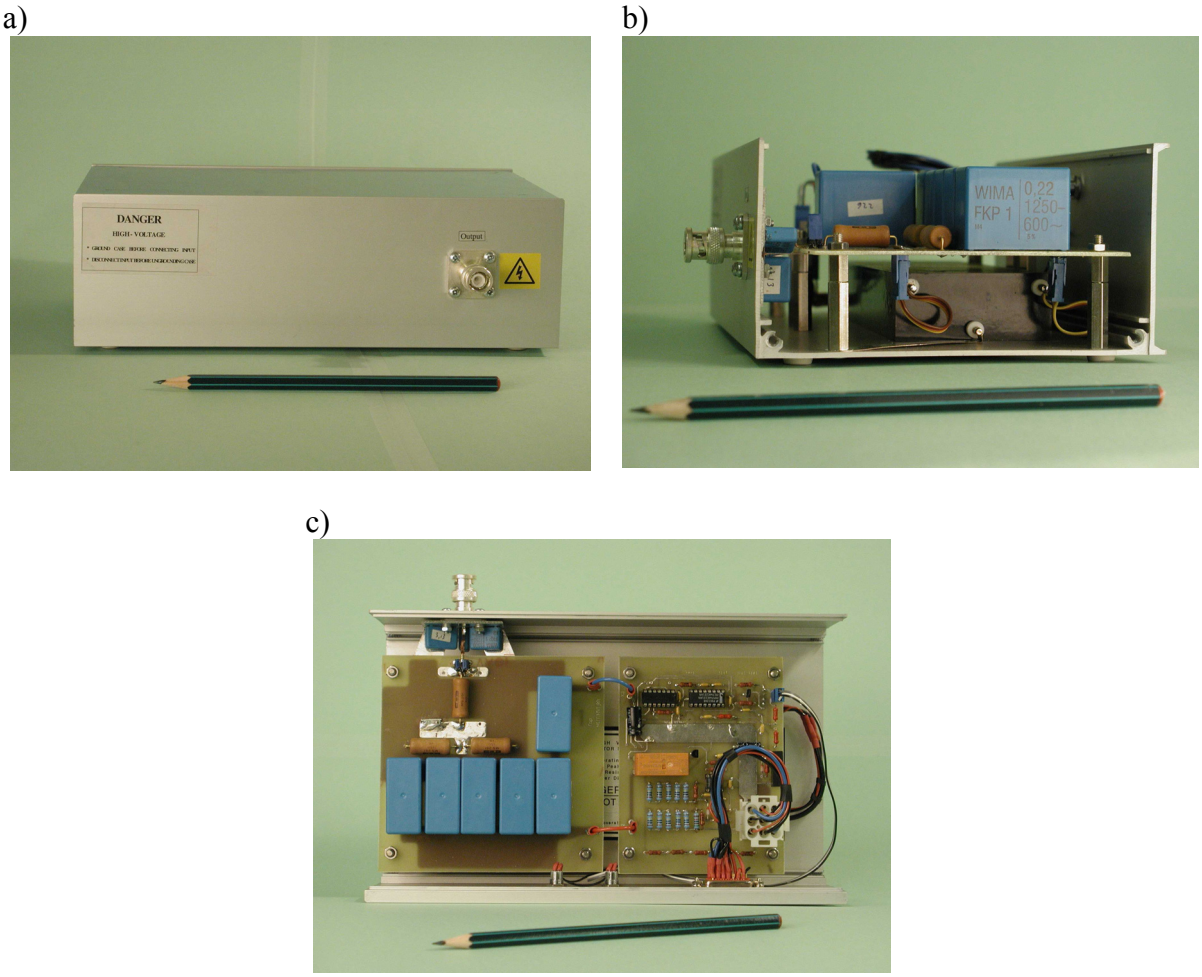

Figure 23 Low impedance calibrator head.
a) Outside view
b) Side view, showing the switch under the PC board
c) From top, the impulse components on the left and control circuits on the right side of the PC board.

6.3.1 Stray inductance

The layout of the impulse circuit is designed to minimize inductance of the loop formed by C_S, the switch, R_D and C_B. The components are of low inductance type, but regardless of that the stray inductance still has influence on the impulse shape. The main influence of stray inductance is the shortening of the front time. For example 100 nH increase in inductance shortens T_1 by 1,3%. The effect of the same inductance increase on U_P and T_2 are –0,05% and 0,07%.

6.3.2 FET switch

As mercury switches with no bounce were not found for voltages above 300 V, an alternative solution had to be found. The earlier prototypes built by Aro and the author used thyristor [24] and IGBT based [2] designs of semiconductor switches. The measured current-voltage characteristics of these switches are shown in Figure 24. The figure also shows the measured characteristics of the commercial switch chosen for this design. It is a commercial FET module (Behlke GmbH, type HTS 21-50), which has several FETs connected in series and in parallel. The control side of the module is galvanically isolated from the high voltage terminals. The main specifications of the switch are shown in Table 19.

6.3.3 Capacitors

Ceramic capacitors could not be used in the low impedance calibrator, because of the higher voltage withstand and capacitance value requirements. Metal film capacitors with polypropylene foil insulation were selected, as they were considered to represent the most appropriate compromise among size, voltage withstand, and stability. The major specifications are shown in Table 20. Using metal foil electrodes ensures good pulse-withstand properties, and the polypropylene insulation gives relatively small size with moderate temperature coefficient.

Table 19 Main specifications of the FET switch module.

Operating voltage range	0 – 2000 V
Galvanic isolation	10 kV
Maximum peak current	500 A
Static on state resistance	0,3 Ω
Maximum off state current	50 μA_{DC}
Turn-on delay time	140 ns
Typical turn-on rise time	15 ns
Coupling capacitance (HV to control)	24 pF
Dimensions	178x64x27 mm^3
Weight	530 g

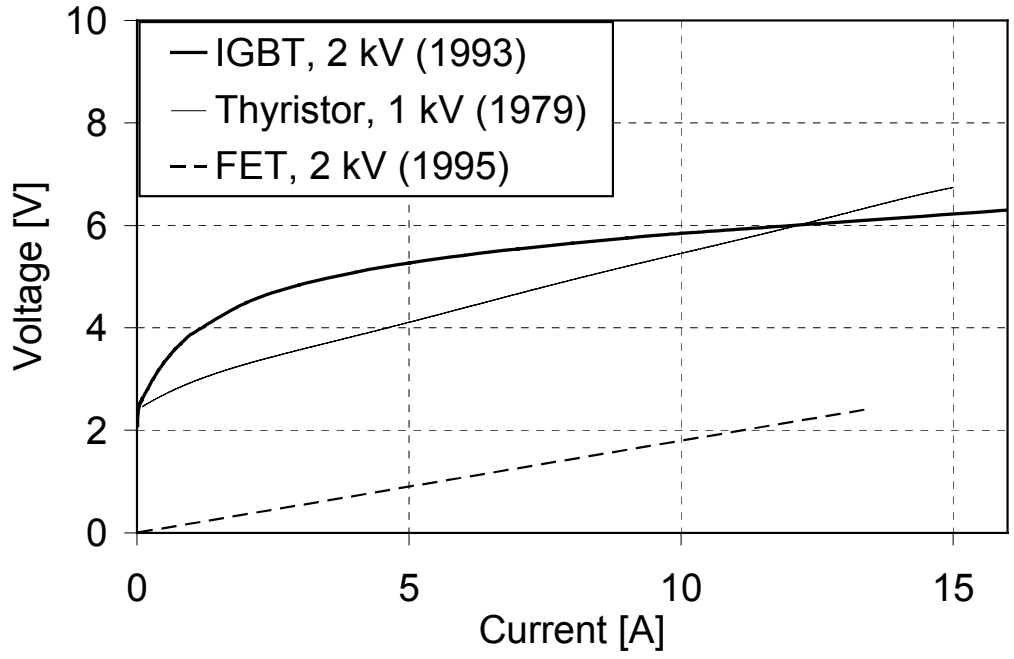

Figure 24 Current-voltage characteristics of the semiconductor switches used in calibrator prototypes.

The voltage coefficient was additionally checked, and the change of capacitance from 10 V and 600 V (r.m.s., 50 Hz) was +0,05% for a 3,3 nF capacitor and +0,33% for a 220 nF one. Four 220 nF capacitors, with an additional series connection of two, are connected in parallel to make a nominal value of 990 nF for C_S and three 3,3 nF capacitors in parallel to have a nominal value of 9,9 nF for C_B.

The capacitance values were checked several times, and the results are shown in Figure 18.

6.3.4 Resistors

For this application, resistors with good pulse withstand characteristics were required. If the stability of the components were not be of high priority, the standard selection for pulse resistor, i.e. carbon mass resistor, would have been ideal. However, as carbon mass resistors betray high temperature and humidity dependencies, they could not be used here.

When a resistor is used for pulse applications, where the pulse width is only microseconds, the resistive material must be able to absorb the energy without

overheating. Transfer of heat from the resistive material to the surroundings is a far slower process that takes place after the pulse has gone. Practically none of the manufacturers of the film resistors gives specifications for energy-withstand for pulse use.

A number of low inductance film resistors were tested with repetitive lightning impulses, and the specifications for the resistor chosen (Caddock Inc., type MS281) are shown in Table 9. Two 150 Ω resistors are connected in parallel to have 75 Ω for R_E, and a single 50 Ω resistor is used for R_D.

The resistance values were checked a number of times, and the results are shown in Figure 26.

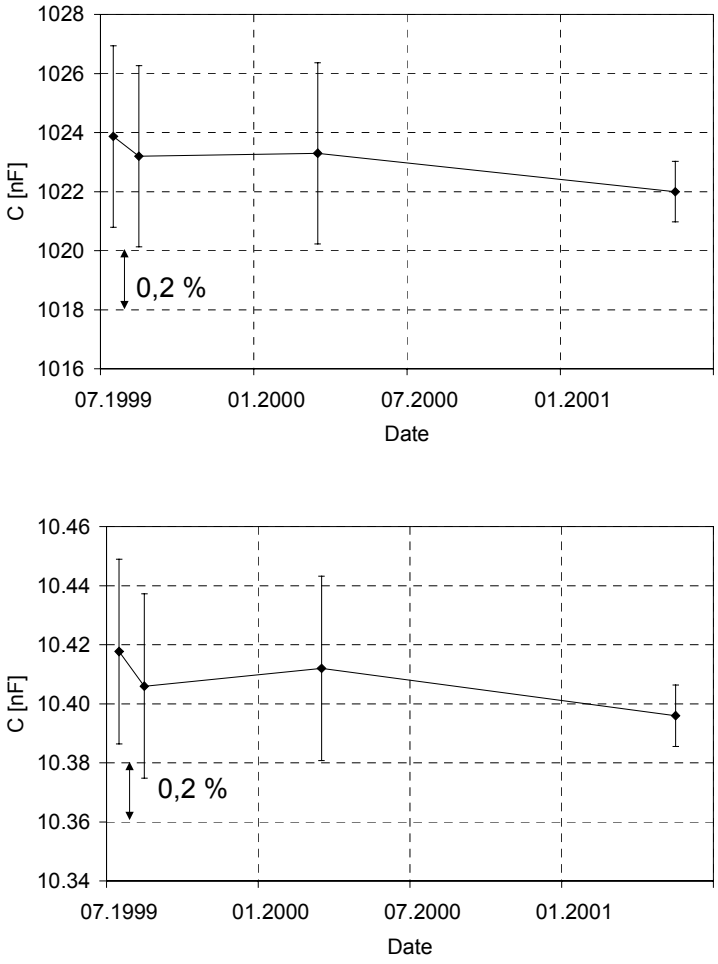

Figure 25 The stability of the capacitors used in the low impedance calibrator. The samples show the calibration results of C_S (top) and C_B (bottom).

Table 20 Main specifications of the capacitors used in the low impedance calibrator.

Type	Metal film capacitors
Capacitance values	3,3 nF / 220 nF
Dielectric	Polypropylene foil
Temperature coefficient	- 300 ppm/K
Tolerance	± 10%
Dissipation factor	≤ 30 x 10^{-3} @ 1 kHz
Voltage gradient	11200 / 3100 kV/µs
Rated voltage	1250 V_{DC}
Proof voltage	2500 V, 2 s

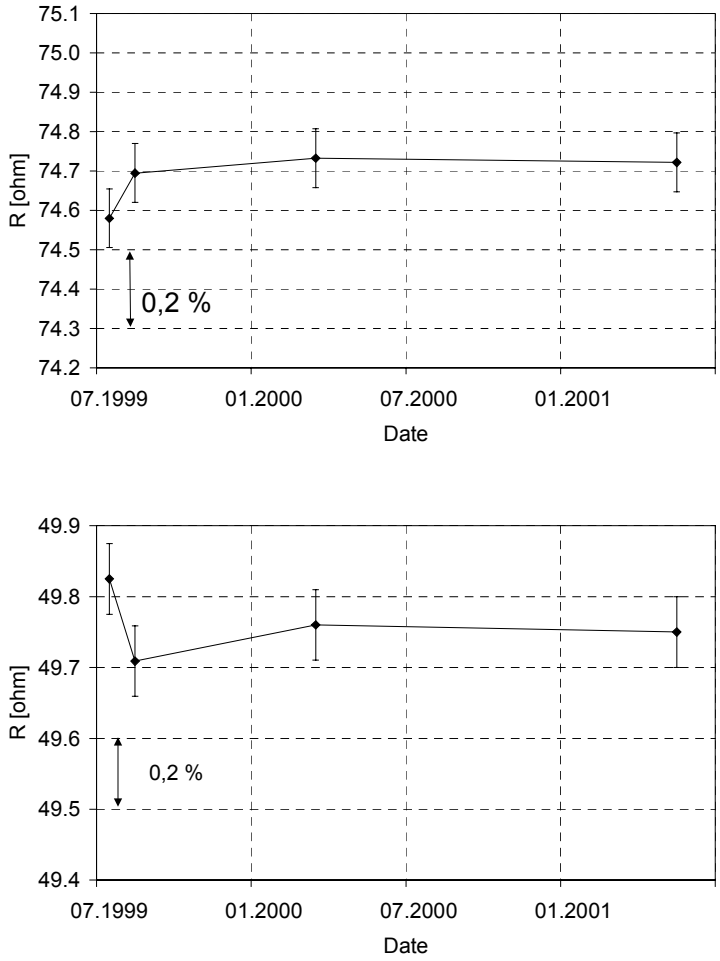

Figure 26 The stability of the resistors used in the low impedance calibrator. The samples show the calibration results of R_E (top) and R_D (bottom).

6.4 Uncertainty analysis

Using the sensitivity coefficients and the uncertainty estimates for each of the components, the uncertainty budgets can be made in a similar way as for the high impedance design (see Section 5.3). Two additional sources for uncertainty are introduced, resistance of the switch and stray inductance of the impulse circuit. The uncertainty budget for is shown in Table 22.

Table 21 Main specifications of the resistors used in the low impedance calibrator.

Type	Power film resistor
Resistance values	50 Ω and 150 Ω
Temperature coefficient	± 50 ppm/K
Tolerance	± 1%
Max. working voltage	2000 V
Max. overload voltage	3000 V
Rated power	8 W

Table 22 Uncertainty budget for the low impedance calibrator head.

LI 1,56/60, low impedance			**Uncertainty budget for peak value (U_P)**		**Uncertainty budget for front time (T_P)**		**Uncertainty budget for time to half value (T_2)**	
Quantity (Component)	Nominal value	Uncert. (k=2)	Sensitivity	Contrib. to uncert.	Sensitivity	Contrib. to uncert.	Sensitivity	Contrib. to uncert.
		%	% / %	%	% / %	%	% / %	%
Capacitance (C_S)	990 nF	0,3	0,04	0,011	0,08	0,023	0,94	0,282
Capacitance (C_B)	9,9 nF	0,5	-0,04	0,018	0,93	0,463	0,06	0,030
Resistance (R_E)	75 Ω	0,1	0,03	0,003	0,07	0,007	0,95	0,095
Resistance (R_S)	0,18 Ω	10	-0,002	0,024	0,004	0,037	0,002	0,024
Resistance (R_D)	50 Ω	0,1	-0,03	0,003	0,94	0,094	0,05	0,005
Inductance (L_S)	250 nH	100	0,0003	0,031	-0,01	0,947	-0,001	0,055
Capacitance (C_L)	40 pF	50	-0,00014	0,01	0,004	0,178	0,0002	0,011
Resistance (R_L)	1 M Ω	5	0,00005	0,0002	0,0001	0,0003	0,0001	0,0004
Voltage (U_C)	100 V	0,02	1,00	0,02				
Overall uncertainty (k=2)				**0,05**		**1,07**		**0,31**

6.5 Verification of software

The reliability of the software was verified by comparison with a circuit simulation program (see section 4.2.1). The differences between the direct calculation and circuit simulation were approximately two orders of magnitude lower than the dominating sources of uncertainty. Because of the good match, the uncertainty originating from the calculation in the software was left out from the uncertainty budget.

7 Results

This chapter gives four examples of the use of the calibrator. All four examples are extracted from the results of an international intercomparison.

In that project HUT prepared a transfer reference system for the comparison of impulse measurement systems. The principal components of the transfer reference system are a calculable impulse voltage calibrator, a digitiser and a resistive impulse voltage divider. The emphasis in the intercomparison project is on high voltage comparison (first results have already been published, see [31, 34-36]).

Each participant was instructed to perform a system calibration on low voltage levels before taking comparison measurements. These calibrations were repeated subsequent to the comparison session.

The following examples are derived from the system calibrations performed by 19 laboratories during the period from June 1999 to September 2001:

1. Series of digitiser calibrations: the transfer digitiser was calibrated 51 times using the transfer calibrators over a period of 27 months. The results show the stability and reliability of both the digitiser and calibrator.
2. Comparison of calibrator heads: one low impedance (1,56/60) and two high impedance (0,84/60 and 1,56/60) calibrator heads of the transfer calibrator are used to calibrate a digitiser. Results of these three calibrations agree well within the estimated uncertainties.
3. Comparison with another National Metrology Institute: during the measurements in Australia, CSIRO compared their own calculable impulse calibrator with the transfer calibrator. Results of lightning impulse comparison on 10 V level are presented. The results agree within their estimated combined uncertainties.
4. Impulse calibration of a resistive lightning impulse voltage divider: impulses (peak value c. 800 V) are delivered from the low impedance transfer calibrator into the transfer divider with a scale factor of c. 11000. The impulses from the divider are measured using the transfer digitiser, which is calibrated using a high impedance transfer calibrator.

7.2 Example 1: Series of calibrations of a digitiser

A digitiser is being circulated within the major high voltage laboratories of the world as part of a comparison project. This digitiser is calibrated by each participating laboratory using a calibrator described in this thesis once when the system arrives at the laboratory, and again before it leaves for the next laboratory. These calibrations have yielded information on the long time stability of both the calculable calibrator and the circulating digitiser. By the end of 2001 19 laboratories had recorded comparison measurements and 51 calibrations of the digitiser had been performed. The digitiser has 10-bit resolution and a sampling rate of 75 MS/s.

An example involving two sets of data is shown in Figure 27. One is gathered using positive impulses and the other using negative. Each point is an average result of 20 impulses. The two sets of data fall well together, showing that there are no polarity dependent effects.

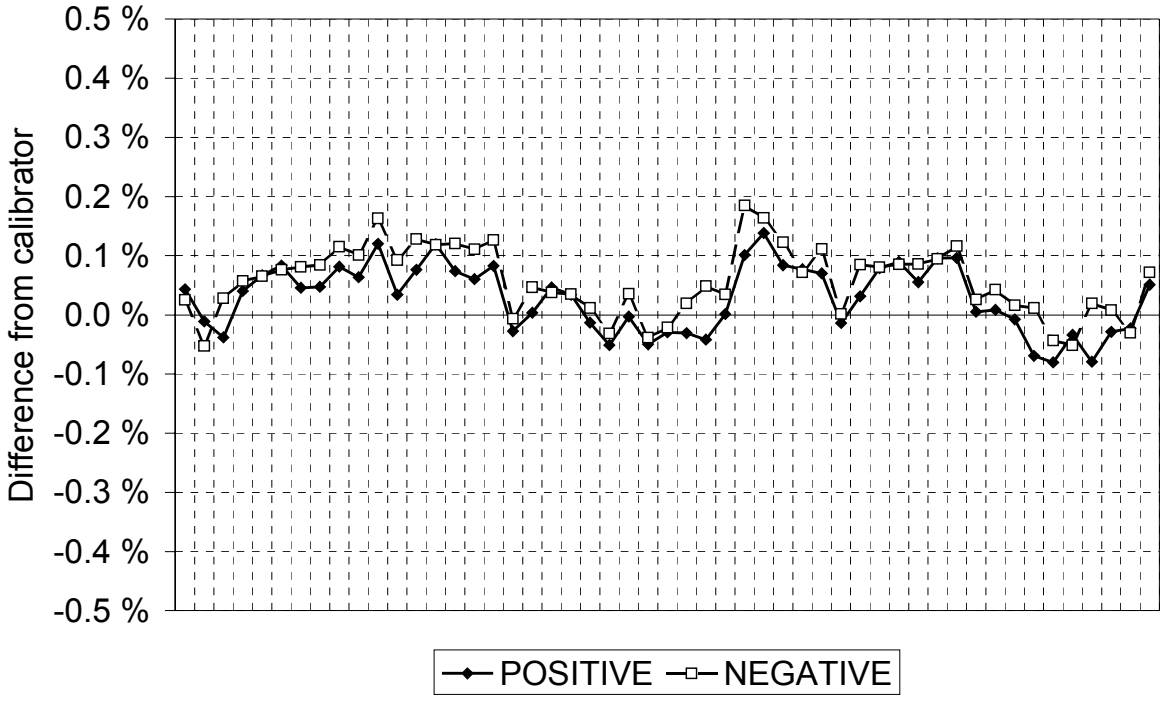

Figure 27 Peak value calibration results of a 10-bit digitiser during a period from June 1999 to September 2001. Peak value of 0,84/60 impulses was approximately 36 V. Estimated uncertainty of each measured point is 0,1% (k=2).

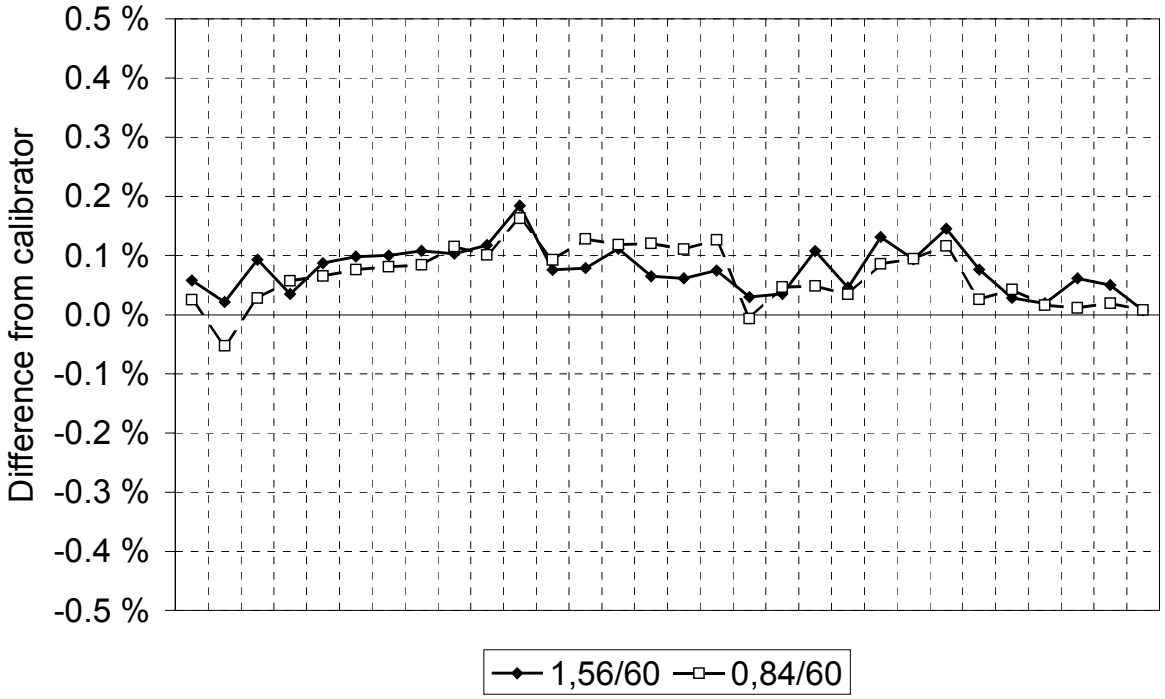

Figure 28 Peak value calibration results of a 10-bit digitiser using two impulse shapes (0,84/60 and 1,56/60) between June 1999 and September 2001. Peak value of positive impulses was approximately 36 V. Estimated uncertainty of each measured point is 0,1% (k=2).

The results obtained by two different calibrator heads, having different front times, agree (Figure 28). Both calibrators have been independently calibrated by capacitance and resistance measurements. The agreement between the two calibrators is clearly within the 0,1% resolution of the digitiser.

7.3 Example 2: Comparison between calibrator heads

One channels of a 10 bit digitizer was calibrated using three calibrator heads. The calibration was performed using both positive and negative impulses with two high impedance calibrators that produced impulse shapes 0,84/60 and 1,56/60 µs. The third calibrator was a low impedance type, having an impulse shape of 1,56/60, and was capable of producing only positive impulses.

The digitizer has 24 ranges, the full scale deflection (f.s.d.) ranges from 10 V to 1280 V. The impulse amplitude was 90% of f.s.d. for all ranges except 1280 V, where the impulse peak value was 1000 V.

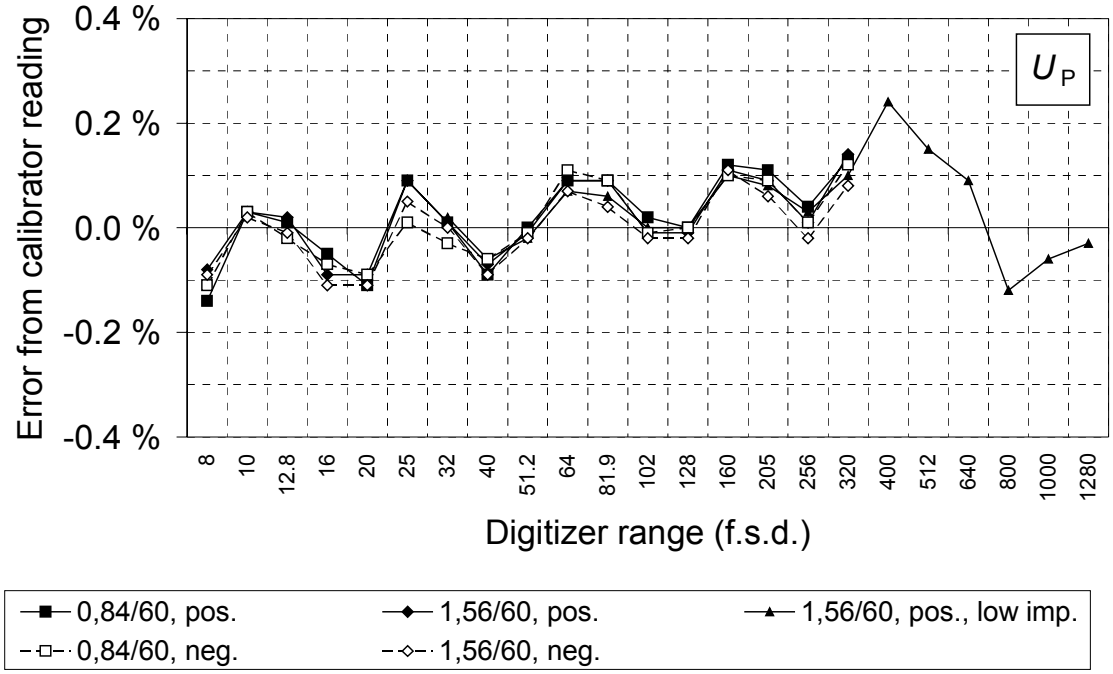

Figure 29 Peak value calibration results of a 10-bit digitiser. Calibration was performed using three calibrator heads. The estimated uncertainty of each measured point is 0,1% (k=2).

The sampling rate of the digitizer was 100 MS/s, and the corresponding sampling interval 10 ns. The sampled data was filtered using a low pass filter with –3dB cut-off frequency of 15 MHz.

7.3.1 Peak value

Results of the peak value calibration are shown in Figure 29. In all ranges all five calibrations agree within the 0,1% resolution of the digitiser. The results show that the digitiser ranges were well adjusted; the systematic errors are only few least significant bits, from -0,05% to 0,25%. Baseline is averaged from samples before the onset of the impulse, and the peak is the maximum value of the filtered data.

7.3.2 Front time

The front time (T_1) values were calculated from the sampled data using linear interpolation. The results of T_1 calibration presented in Figure 30 show systematic error of approximately 1%. The results further reveal a subtle polarity

effect, which produces approximately 0,5% larger error when negative impulses are measured.

For the lower T_1 (0,84 µs) the corresponding time interval between the 30% and 90% points is approximately 500 ns, which corresponds to 50 samples with the used 10 ns sample rate. The errors found correspond to a time interval of less than one sample.

The impedance parameter for the low impedance calibrator was adjusted to give identical readings with the high impedance calibrators between 10 V and 300 V.

7.3.3 Time to half value

A systematic polarity effect can similarly be seen in the time to half value (T_2) calibration results in Figure 31. In this case, the 0,5% - 0,8% differences between the positive and negative calibration results can be seen. The reason for this may be either the creeping step response of the digitiser or the offset circuit used to shift the dc level for measurement of negative voltages. At the 50% level on the impulse tail the gradient of the curve is low, and small changes in the amplitude invoke larger changes in the time measurement.

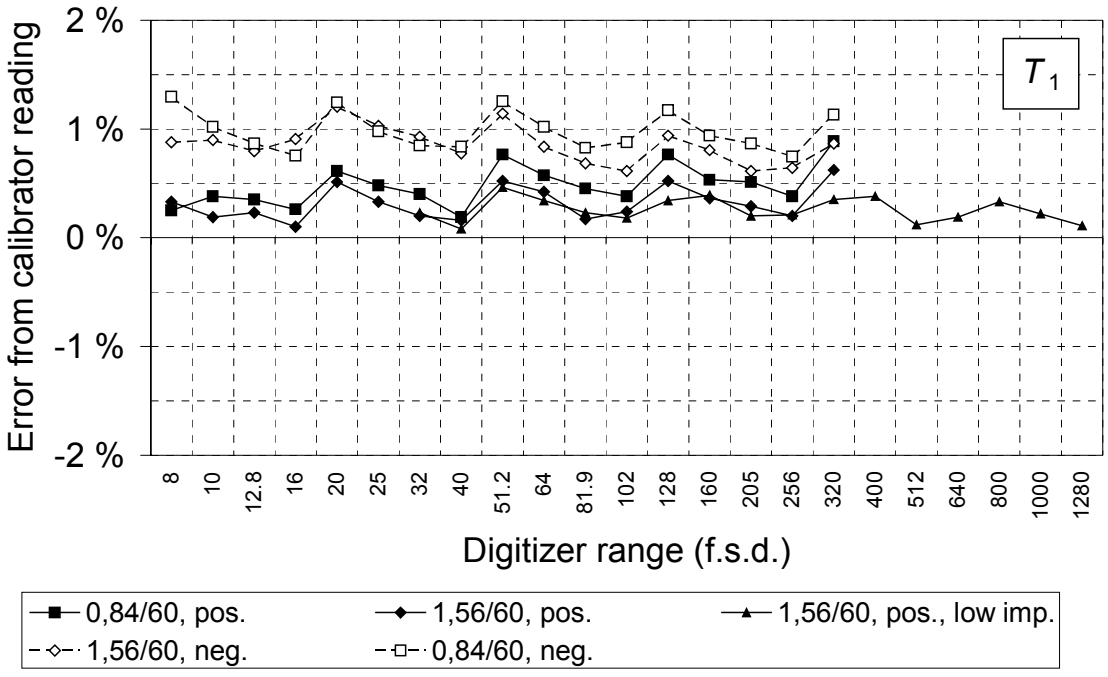

Figure 30 Front time calibration results of a 10-bit digitiser. Calibration was performed using three calibrator heads. The estimated uncertainty of each measured point is 0,5% (k=2).

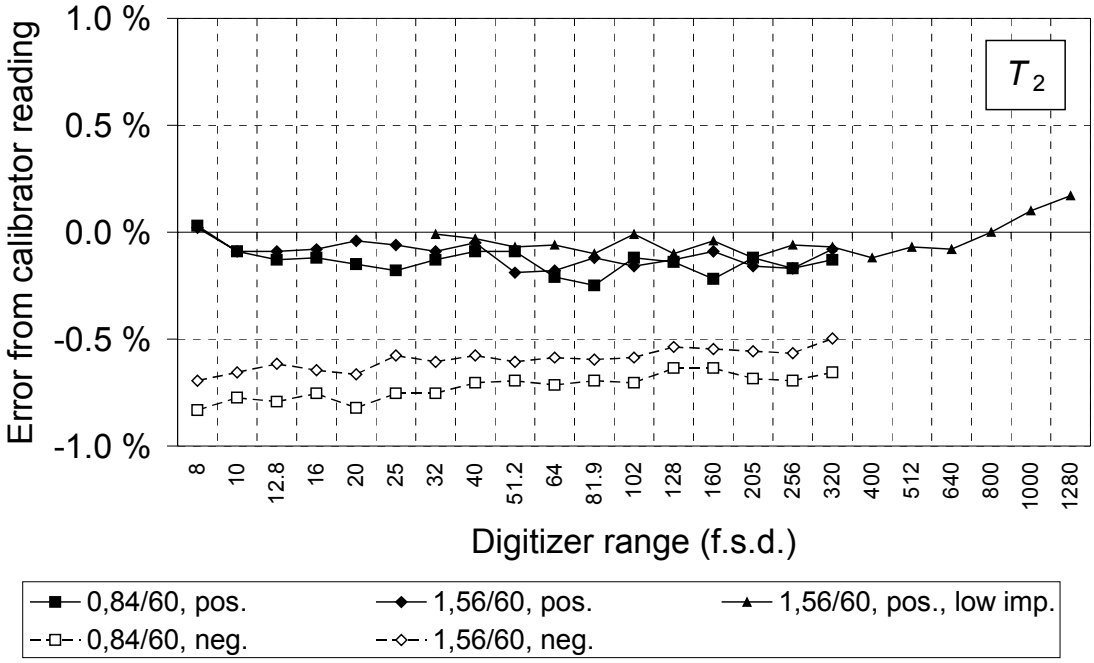

Figure 31 Time to half value calibration results of a 10-bit digitiser. Calibration was performed using three calibrator heads. The estimated uncertainty of each measured point is 0,5% (k=2).

7.4 Example 3: Comparison with CSIRO

The Australian participant of the worldwide intercomparison, CSIRO National Measurement Laboratory, has also published papers on calculable impulse calibrators [6, 26]. During the intercomparison project, they made an indirect comparison between the calibrator described in this thesis and their calibrator, based on a same principle (see Section 3.2). Both calibrators were used to calibrate the same digitiser, and the results were compared.

The results of the comparison on 10 V level are presented here. The two high impedance LI calibrator heads with impulse shapes 0,84/60 and 1,56/60 were used to apply both positive and negative impulses.

Measurement results for peak value comparison are shown in Figures 32 to 34. The estimated combined uncertainty for each quantity (U_P, T_1 and T_2) is obtained from

$$u_{\text{comb}} = \sqrt{u_{\text{std}}^2 + u_{\text{hut}}^2 + u_{\text{csiro}}^2}\,, \tag{28}$$

where u_{std} is twice the standard deviation of the comparison results, u_{hut} the estimated uncertainty of HUT calibrator (k=2) and u_{csiro} the corresponding value for CSIRO calibrator. The values for u_{hut} and u_{csiro} are summarised in Table 23. The standard deviation was not the dominating source of uncertainty in any of the measurements.

The measured values agree within the estimated combined uncertainty on all peak value and T_2 measurements; no clear systematic disagreements can be found on these measurements.

Front time values show approximately 1% systematic disagreement, which is, however, in most cases within the estimated combined uncertainty.

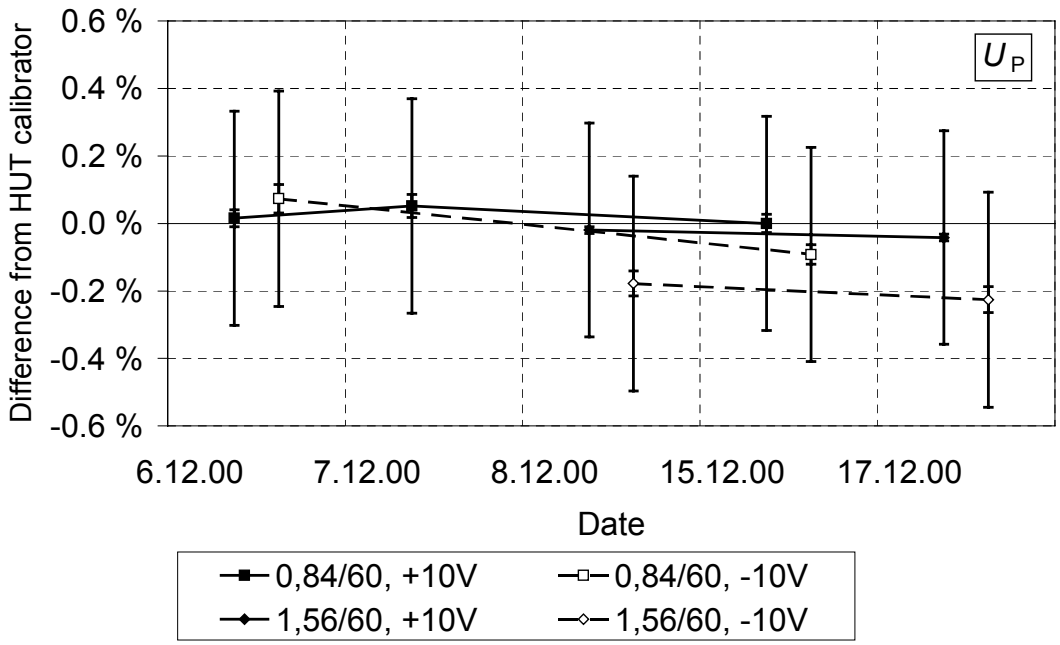

Figure 32 Peak value results of LI comparison with CSIRO. Inner error bars show one standard deviation of the comparison results, and outer error bars the estimated combined uncertainty of the comparison (k=2).

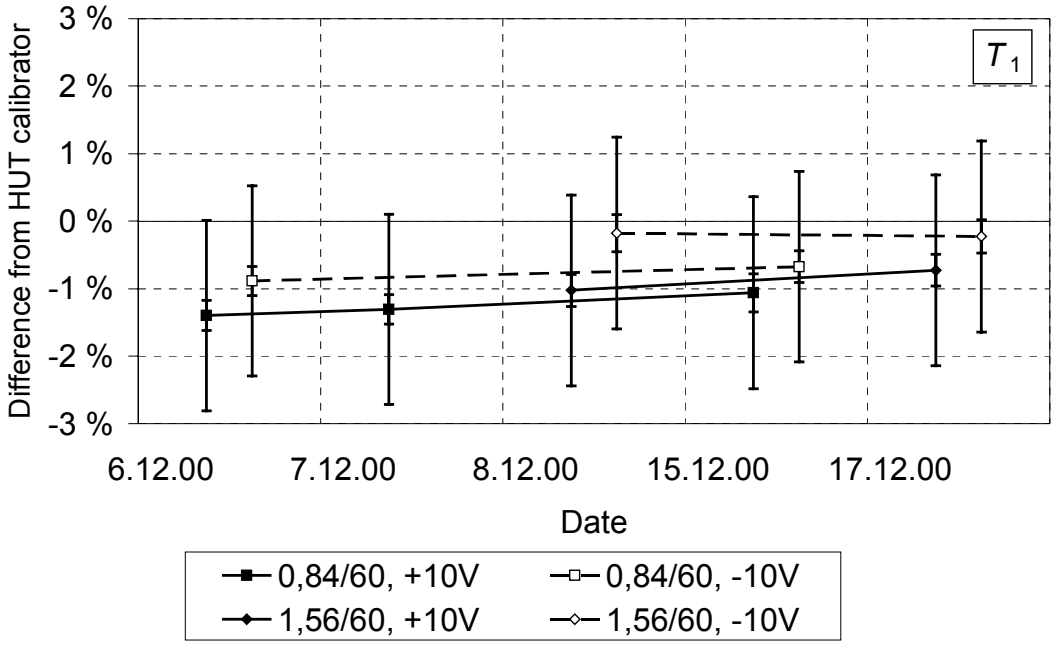

Figure 33 Front time results of LI comparison with CSIRO. Inner error bars show one standard deviation of the comparison results, and outer error bars the estimated combined uncertainty of the comparison (k=2).

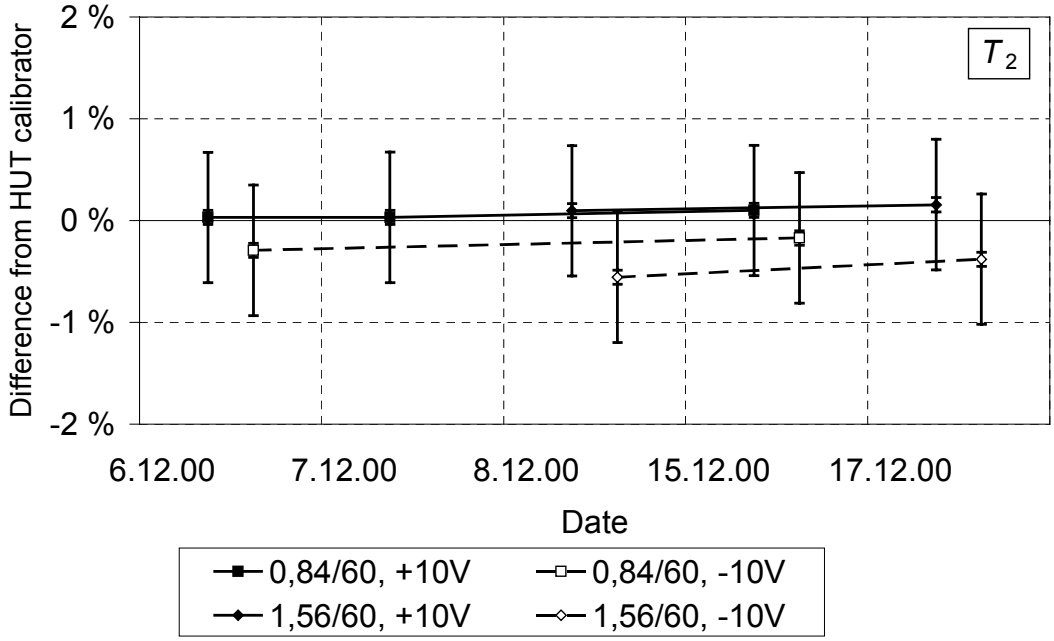

Figure 34 Time to half value results of LI comparison with CSIRO. Inner error bars show one standard deviation of the comparison results, and outer error bars the estimated combined uncertainty of the comparison (k=2).

Table 23 Estimated expanded uncertainties for HUT calibrator and CSIRO measuring system.

	U_P	T_1	T_2
u_{hut}	0,1%	0,5%	0,5%
u_{csiro}	0,3%	1,3%	0,4%

7.5 Example 4: Impulse calibration of a resistive divider

As part of the low voltage checks in the worldwide intercomparison, participants were asked to calibrate the transfer divider scale factor both using direct voltage and the low impedance transfer calibrator. Calibrations performed between September 1999 and February 2000 are summarised in Figure 35.

The direct voltage scale factor measurement was performed on two voltage levels using both positive and negative voltages. The average of these four measurements was used as the result of dc calibration.

The impulse scale factor was measured using the transfer calibrators. The low impedance calibrator was used to deliver impulses with accurately known peak voltage $\hat{u}_i$. The peak value of these impulses was approximately 800 V.

A digitiser was used to measure the output of the divider, $\hat{u}_o$. The scale factor of the divider was approximately 11000; thus the output voltage was approximately 80 mV. The digitiser range used for measuring the 80 mV signal was calibrated using a high impedance calibrator.

The impulse scale factor can now be determined as the ratio $\hat{u}_i / \hat{u}_o$, where both peak values are traceable to the transfer calibrators. Good agreement between the measured dc and scale factors was found, which in this case was expected, as the divider used as transfer reference was known to behave well when full lightning impulses are measured.

Similarly, the impulse calibrators can also be used to verify errors introduced by the divider to the time parameters. The low impedance calibrator gives the time parameters delivered into the divider input, and the high impedance calibrator can be used to cancel out the errors caused by the digitiser. An example of this approach is presented in Table 24.

Table 24 Estimation of errors introduced to time parameters by the transfer divider.

	T_1	T_2
Divider input, nominal values	1,56 µs	60 µs
Divider output	+1,3%	+0,2%
Digitiser errors	+1,0%	+0,4%
Divider output, digitiser errors compensated	**0,3%**	**-0,2%**

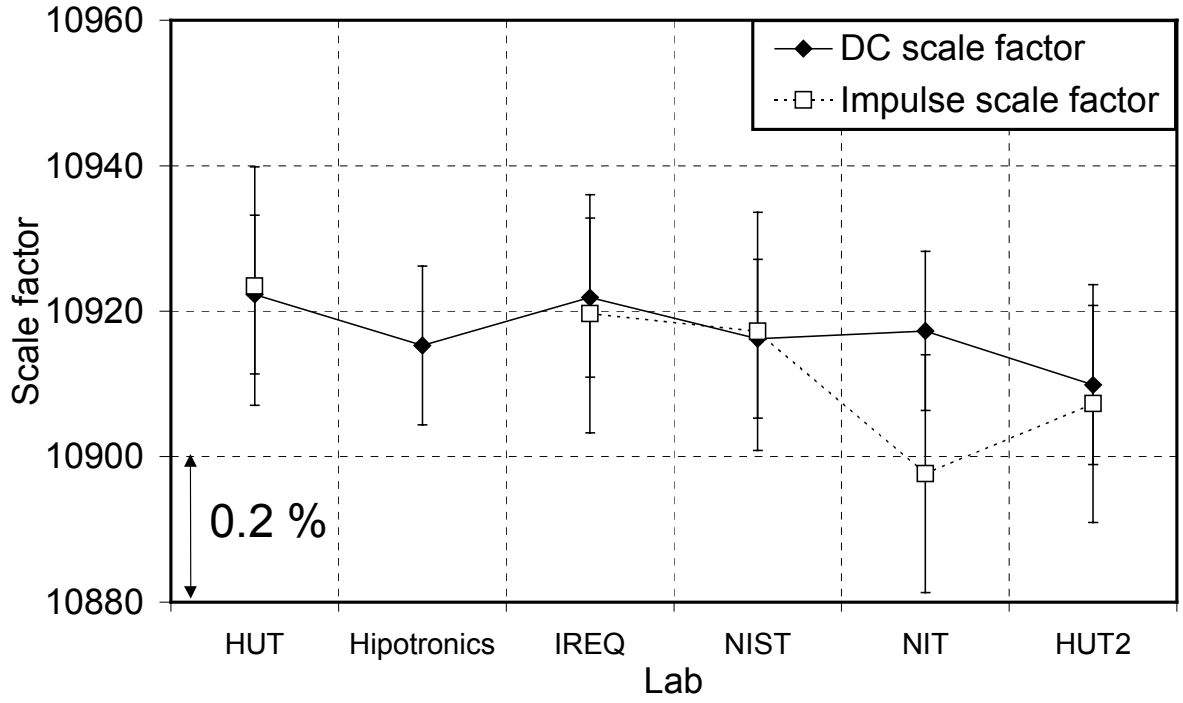

Figure 35 Comparison of measured DC and impulse scale factors of the transfer divider. The error bars show the estimated uncertainties for both methods, 0,1% for dc and 0,15% for impulse scale factor.

8 Conclusions and future work

8.2 Conclusions

The principle of a calculable impulse calibrator is presented in this thesis. The design, construction and performance of two types of calibrator are described, and the main sources of uncertainty are analysed.

The calibrators have proven to be accurate and reliable, and they have been used as transfer reference in a large international comparison of the highest level of accuracy.

Uncertainty budgets are presented for each relevant parameter, i.e. peak values U_P, front time T_1 (for LI) or time to peak (for SI), and time to half value T_2. These uncertainty budgets are based on traceable calibration of the resistance, capacitance and voltage.

The accuracy of the calibrators has been verified by means of comparison between National Metrology Institutes.

The applicability of the method has been demonstrated by examples of digitiser calibration, and by comparison. The following conclusions can be made:

- The primary reference of both lightning and switching impulse parameters can be based on the calculable impulse calibrator. The method has a direct and clear traceability chain to SI quantities.
- The uncertainty achieved using the calculable impulse voltage calibrator is significantly lower than using any other method. The correctness of the uncertainty analysis is supported by comparison with independent realisation of a system based on the same principle.
- The precision of this calibration method is adequate for the calibration of even the most accurate instruments.
- In high-voltage impulse measurements, the gap between the uncertainties required for testing and available for calibration of instruments is narrow. The use of calculable impulse calibrator clearly widens the gap for calibration of measuring instruments.

The calibrators described in this thesis have been used to calibrate many devices. The following general observations based on the experience with these calibrations can be made:

- The calibrator can additionally be used for calibration of a high-voltage divider. The impulse calibration can reveal measurement errors caused by frequency dependent effects, which can not be noticed by direct voltage calibration. In addition to the impulse scale factor, information on the errors in time parameter measurement can be obtained.
- The experience with the calibrator indicates that the main problems with the accuracy of high-voltage impulse measurements are experienced with the calibration of the digital recorder. Creeping response of the digitiser to a step can render the scale factor calibration with direct voltage invalid, and occasionally produces considerable errors in time parameters. These calibration problems are multiplied, as different ranges and channels in one recorder frequently behave in different ways.

8.3 Future work

One possible way to proceed is to try to reduce the uncertainties. The accuracy limit of this method has not been dealt with in this work. The method could still be pushed for lower uncertainties by concentrating on the calibration on the components and measurement of the charging voltage.

Another direction for the future work could be the calibration of chopped impulses. The definitions of the parameters of chopped impulses are given in standard IEC 60060-1. One of them is time to chopping, which can range from approximately 500 ns to several microseconds. An additional switch is required for shorting the output of the generator output to ground. The problems to be solved are:

- The timing between the two switches required.
- The components should withstand shorting of the output.
- The switch connected in parallel with the output either adds a load, which is difficult to model (FET with voltage dependent capacitance), and impossible to time accurately (mercury-wetted relay).

Trials were made with a FET switch applied for to a low impedance calibrator. Because of problems in timing and modelling the idea was not pursued further at that time.

The third option is to make a calculable calibrator for some tens of kilovolts. Solid-state switches are commercially available, and by careful selection of calibrator components and using appropriate model for the circuit, an accurate enough solution might be found.

A fourth area of interest might involve combining the experience gained from this work with the notion of calculating the parameters of a multistage high-voltage generator. There is a good chance that at least the peak value could be calculated accurately enough for calibration work. Potential problems include:

- High-voltage impulse generators tend to produce oscillations, particularly at the front of the impulse. The oscillations are caused by the stray inductance of the components or the complete circuit. To avoid these oscillations either an impulse generator with low stray inductance should be selected or long front times should be considered.
- The switching element used in high-voltage impulse generators is sphere-gap. The behaviour and voltage-loss of multiple gaps in series must be taken into account.

9 References

[1] CIGRE Task Force 33.03 3.2, (J. Rungis, R. Hughes, T. McComb, M. Aro, R. Diaz, F. Garnacho, J. Hällström, V. Jaroslawski, J. Kuffel, W. Larzelere, M. Muhr, P. Munhoz Rojas, G. Rizzi, B. Sacepe, and K. Schon), "Use of low voltage calibrators in impulse voltage measurement," *Electra*, pp. 83-109, 2000.

[2] Jari Hällström, Martti Aro, and Mika Kivelä, "Lightning impulse calibration circuit for voltages up to 1800 V," Proceedings of the 8th International Symposium on High Voltage Engineering, pp. 423-426, Yokohama, 1993.

[3] Jari Hällström, Martti Aro, Viktor Kiseliev, and Vitali Jaroslawski, "Comparison of three methods for calibrating lightning impulse voltage measuring devices," Proceedings of the High Voltage Measurement and Calibration, pp. P4.1 - P4.9, Arnhem, 1994.

[4] Jari Hällström and Martti Aro, "Practical experience with calculable impulse voltage calibrator," Proceedings of the Measurements and Calibration in High Voltage Testing, pp. 2.6.1. - 2.6.10., London, 1998.

[5] Martti Aro and Yrjö Rantanen, "Precision impulse voltage calibrator," Proceedings of the 3rd International Symposium on High Voltage Engineering, paper 42.11, Milan, 1979.

[6] Yi Li, Ron Sheehy, and Juris Rungis, "The calibration of a calculable impulse voltage calibrator," Proceedings of the 10th International Symposium on High Voltage Engineering, pp. 45-49, Montréal, 1997.

[7] IEC 61083-1:1991, *Digital recorders for measurements in high-voltage tests, Part 1: Requirements for digital recorders.*

[8] Edmund Kuffel, Walter S. Zaengl, and John Kuffel, *High Voltage Engineering: Fundamentals*, 2nd ed: Newnes, 2000.

[9] "Traceability of measurements," The International Laboratory Accreditation Cooperation (ILAC) ILAC-G2, 54 pages, 1994.

[10] "National and International Needs Relating to Metrology," BIPM, 132 pages, 1998.

[11] IEC 60060-1:1989, *High-voltage test techniques, Part 1: General definitions and test requirements.*

[12] IEC 60060-2:1994, *High-voltage test techniques, Part 2: Measuring Systems.*

[13] IEC 61083-1:2001, *Instruments and software used for measurements in high-voltage impulse tests - Part 1: Requirements for instruments.*

[14] IEC 61000-4-5:1995, *Electromagnetic compatibility (EMC) - Part 4: Testing and measurement techniques - Section 5: Surge immunity tests.*

[15] IEC 60060-2:1962, *High-voltage test techniques.*

[16] IEC 60060-2:1973, *High-voltage test techniques - Part 2: Test procedures.*

[17] Sonja Berlijn, "Influence of lightning impulses to insulating systems," in *Faculty of Electrical Engineering*: Technical University of Graz, 2000, 140 pages.

[18] Sonja Berlijn, Fernando Garnacho, Ernst Gockenbach, Michael Muhr, K. Hackemack, Mats Kvarngren, P. Simón, and P. Werle, "Influence of different lightning impulse shapes on the breakdown behaviour of insulating materials -Proposal for modification of IEC 60060-1," Proceedings of the 12th International Symposium on High Voltage Engineering, pp. 1081-1084, Bangalore, India, 2001.

[19] IEC 60790:1984, *Oscilloscopes and peak voltmeters for impulse tests.*

[20] Alfred Vondenbusch, "Beitrag zur Berechnung von Stoßschaltungen mit zwei Energiespeichern," *Elektrotechnische Zeitschrift Ausgabe A*, vol. 80, pp. 617-622, 1959.

[21] Alfred Vondenbusch, "Ein allgemeines Berechnungsverfaren für Stoßschaltungen mit drei voneinander unabhängigen Energiespeichern," in *Fakultät für Machinenwesen und Elektrotechnik*. Aachen: Rheinisch-Westfälischen Technischen Hochschule, 1958, 70 pages.

[22] Friedrich Wilhelm Rutloh, "Der Ausnutzgrad von Stoßspannungsgeneratoren mit drei Energiespeichern," *Elektrotechnische Zeitschrift Ausgabe A*, vol. 90, pp. 633-637, 1969.

[23] Otmar Etzel and Günter Helmchen, "Berechnung der Elemente des Stoßspannungskreises für die Stoßspannungen 1,2/50, 1.2/5 und 1,2/200," *Elektrotechnische Zeitschrift Ausgabe A*, vol. 85, pp. 578-582, 1964.

[24] Martti Aro, "Accuracy of impulse voltage measurements," Proceedings of the Nord-IS, pp. 25:1 - 25:4, Espoo, Finland, 1986.

[25] Dexiang Huang, Huigao Zhou, and Yang Zhang, "Experimental calibration of impulse voltage calibrator," Proceedings of the 7th International Symposium on High Voltage Engineering, pp. 59-62, Dresden, 1991.

[26] Yi Li, Juris Rungis, Terry McComb, and Wolfgang Lucas, "International comparison of a pulse calibrator used in high-voltage impulse calibration," *IEEE Transactions on Instrumentation and Measurements*, vol. 50, pp. 430-435, 2001.

[27] Viktor V. Kiseliev and Vitali N. Jaroslawski, "Reference measuring devices for pulses amplitude up to 1kV," Proceedings of the 7th International Symposium on High Voltage Engineering, pp. 55-58, Dresden, 1991.

[28] Viktor Kiseliev, "A new type of differential meter," Proceedings of the 8th International Symposium on High Voltage Engineering, pp. 411-413, Yokohama, 1993.

[29] Martti Aro, Jorma Elovaara, Matti Karttunen, Kirsi Nousiainen, and Veikko Palva, *Suurjännitekniikka*, 1st edition: Otatieto Oy, 1996.

[30] Magnecraft & Struthers-Dunn, Industrial relays, Edition 102, p. 68.

[31] Jari Hällström and Martti Aro, "Traceability and recognizability of impulse voltage measurements," Helsinki University of Technology, Espoo TKK-SJT-43, 110 pages, 2001.

[32] "Expression of the Uncertainty of Measurement in Calibration," European Co-operation for Accreditation, EA-4/02, 79 pages, 1999.

[33] GUM Workbench, Version 1.2, Metrodata GmbH, 1999.

[34] Jari Hällström, Martti Aro, Yixin Zhang, Bill Larzelere, Jeremy FitzPatrick, Normand Rivest, Louis Lavallée, and Takayuki Wakimoto, "Progress of a worldwide comparison of LI measuring systems - Round

1," Proceedings of the 12th International Symposium on High Voltage Engineering, pp. 1077-1080, Bangalore, 2001.

[35] Marja-Leena Pykälä, Jari Hällström, and Martti Aro, "Traceability and recognizability of impulse voltage measurements - Round two," Helsinki University of Technology, Espoo TKK-SJT-54, 176 pages, 2002.

[36] Marja-Leena Pykälä, Arja Hokkanen, and Jari Hällström, "Lightning impulse measurements, comparison of HUT home systems to circulating system," Helsinki University of Technology, Espoo TKK-SJT-53, 129 pages, 2002.

Appendix A

Basics of uncertainty evaluation

The following overview is adapted from the document "Expression of the Uncertainty of Measurement in Calibration" (EA-4/02) [32]*, published by European co-operation for accreditation.*

1) Type A and Type B uncertainty evaluation

The **Type A evaluation of standard uncertainty** is the method for evaluating uncertainty using the statistical analysis of a series of observations. In this case the standard uncertainty is the experimental standard deviation of the mean that follows from an averaging procedure or an appropriate regression analysis.

Assume that the repeatedly measured input quantity X_i is the quantity Q. With n statistically independent observations ($n > 1$), the estimate of the quantity Q is q, the **arithmetic mean** or the **average** of the individual observed values q_j ($j = 1,2,\ldots,n$)

$$\overline{q} = \frac{1}{n}\sum_{j=1}^{n} q_{\mathrm{j}} .$$

The uncertainty of measurement associated with the estimate q is evaluated according to one of the following methods:

(a) An estimate of the variance of the underlying probability distribution is the **experimental variance** $s^2(q)$ of values q_{j} that is given by

$$s^2(q) = \frac{1}{n-1}\sum_{j=1}^{n}(q_{\mathrm{i}} - \overline{q})^2 .$$

Its (positive) square root is termed **experimental standard deviation**. The best estimate of the variance of the arithmetic mean q is the **experimental variance of the mean** given by

$$s^2(\overline{q}) = \frac{s^2(q)}{n} .$$

Its (positive) square root is termed experimental standard deviation of the mean. The standard uncertainty $u(q)$ associated with the input estimate q is the experimental standard deviation of the mean

$$u(\overline{q}) = s(\overline{q}).$$

(b) For a measurement that is well characterised and under statistical control a combined or **pooled estimate of variance** s_p^2 may be available that characterises the dispersion more reliably than the estimated standard deviation obtained from a limited number of observations. If in such a case the value of the input quantity Q is determined as the arithmetic mean q of a small number n of independent observations, the variance of the mean may be estimated by

$$s^2(\overline{q}) = \frac{s_p^2}{\mathrm{n}}.$$

The **Type B evaluation of standard uncertainty** is the method for evaluating the uncertainty using means other than the statistical analysis of a series of observations. In this case, the evaluation of the standard uncertainty is based on some other scientific knowledge.

Values belonging to this category may be derived from

- previous measurement data;
- experience with or general knowledge of the behaviour and properties of relevant materials and instruments;
- manufacturers' specifications;
- data provided in calibration and other certificates;
- uncertainties assigned to reference data taken from handbooks.

2) Calculation of the standard uncertainty of the output estimate

For uncorrelated input quantities, the square of the standard uncertainty associated with the output estimate y is given by

$$u^2(y) = \sum_{i=1}^{N} u_i^2(y).$$

The quantity $u_i(y)$ (i = 1, 2, …, N) is the contribution to the standard uncertainty associated with the output estimate y resulting from the standard uncertainty associated with the input estimate x_i

$$u_i(y) = c_i u(x_i),$$

where c_i is the **sensitivity coefficient** associated with the input estimate x_i, i.e. the partial derivative of the model function f with respect to X_i, evaluated at the input estimates x_i,

$$c_i = \frac{\partial f}{\partial x_i}.$$

3) Uncertainty budget

Uncertainty budget can be presented as an ordered arrangement of the quantities, estimates, standard uncertainties, sensitivity coefficients, and uncertainty contributions used in the uncertainty analysis of a measurement (see Table A-1).

Table A-1 Schematic of an uncertainty budget presented in tabular format.

Quantity	Estimate	Standard uncertainty	Sensitivity coefficient	Contribution to the standard uncertainty
X_i	x_i	$u(x_i)$	c_i	$u_i(y)$
X_1	x_1	$u(x_1)$	c_1	$u_1(y)$
X_2	x_2	$u(x_2)$	c_2	$u_2(y)$
⋮	⋮	⋮	⋮	⋮
X_N	x_N	$u(x_N)$	c_N	$u_N(y)$
Y	y			$u(y)$

Appendix B

Uncertainty calculation for high impedance calibrator peak value

The peak value of a calculable impulse voltage calibrator is calculated from the component values and charging voltage. This uncertainty estimate is determined for 1 V impulse, but it is valid for voltages from 500 mV to 300 V. It assumes that the load resistance is measured with an uncertainty of less than 0.5% (k=2) and the load capacitance with an uncertainty of less than 5 pF (k=2).

This uncertainty analysis is performed according to EA-4/02 (previously EAL-R2) using GUM Workbench software by Metrodata GmbH.

Model equation:

$C_{Bx}=(1+\alpha_C*\Delta T+u_C)*\upsilon_C*C_B$;
$C_{Sx}=(1+\alpha_C*\Delta T+u_C)*\upsilon_C*C_S$;
$R_{Ex}=(1+\alpha_R*\Delta T+u_R)*R_E$;
$R_{Dx}=(1+\alpha_R*\Delta T+u_R)*R_D$;
$C_2=C_{Bx}+C_L$;
$a=R_{Dx}*R_{Ex}*R_L*C_{Sx}*C_2$;
$b=R_{Dx}*R_L*C_2+R_{Ex}*R_L*C_2+R_{Dx}*R_{Ex}*C_{Sx}+R_{Ex}*R_L*C_{Sx}$;
$c=R_{Dx}+R_{Ex}+R_L$;
$d=C_{Sx}*R_{Ex}*R_L$;
$g=-(b+\mathrm{sqrt}(b*b-4*a*c))/(2*a)$;
$h=-(b-\mathrm{sqrt}(b*b-4*a*c))/(2*a)$;
$t_P=\ln(g/h)/(h-g)$;
$\eta=d*(\exp(g*t_P)-\exp(h*t_P))/(a*(g-h))$;
$U_P=\eta*U_C$

List of quantities:

Quantity	Unit	Definition
C_S	F	Measured tail capacitance
C_B	F	Measured front capacitance
R_E	Ω	Measured tail resistance
R_D	Ω	Measured front resistance
C_L	F	Measured load capacitance
R_L	Ω	Measured load resistance
U_C	V	Measured tail capacitor charging voltage
υ_C		Voltage dependence of capacitors C_B and C_S

Quantity	Unit	Definition
α_C	K^{-1}	Front and tail capacitor temperature coefficient
α_R	K^{-1}	Front and tail resistor temperature coefficient
ΔT	K	Deviation from the component calibration temperature
u_C		Correction of second order terms of (α_C * ΔT)
u_R		Correction of second order terms of (α_R * ΔT)
C_{Sx}	F	Interim result
C_{Bx}	F	Interim result
R_{Ex}	Ω	Interim result
R_{Dx}	Ω	Interim result
C_2	F	Interim result, sum of parallel C_B and C_L
d		Interim result
a		Interim result
b		Interim result
c		Interim result
g		Interim result
h		Interim result
t_P	s	Calculated time of peak
η		Efficiency factor
U_P	V	Peak voltage

C_S:

Type A
Method of observation: Direct

Number of observation: 4

No.	Observation
1	$18.40 \cdot 10^{-9}$
2	$18.39 \cdot 10^{-9}$
3	$18.385 \cdot 10^{-9}$
4	$18.392 \cdot 10^{-9}$

Arithmetic mean: $18.3918 \cdot 10^{-9}$ F

Pooled Standard deviation: 0.25 %

Standard uncertainty: $23.0 \cdot 10^{-12}$ F

Pooled Degrees of freedom: 2

CALIBRATED VALUE: The tail capacitor is calibrated by measuring its capacitance with a capacitance bridge. The connection between R_D and C_B is opened, the relay is closed, and the capacitance measured from the terminals of the capacitor. Uncertainty of each calibration is 0.1% (k=2).

***C_B*:**

Type A

Method of observation: Direct

Number of observation: 4

No.	Observation
1	$1.289 \cdot 10^{-9}$
2	$1.287 \cdot 10^{-9}$
3	$1.2875 \cdot 10^{-9}$
4	$1.2892 \cdot 10^{-9}$

Arithmetic mean: $1.288175 \cdot 10^{-9}$ F

Pooled Standard deviation: 0.15 %

Standard uncertainty: $966 \cdot 10^{-15}$ F

Pooled Degrees of freedom: 2

CALIBRATED VALUE: The front capacitor is calibrated by measuring its capacitance with a capacitance bridge. The connection between R_D and C_B is opened and the capacitance measured from the output BNC. The uncertainty of each calibration is 0.5% (k=2).

***R_E*:**

Type A

Method of observation: Direct

Number of observation: 4

No.	Observation
1	4306.3
2	4306.1
3	4306.4
4	4306.7

Arithmetic mean: 4306.38 Ω

Pooled Standard deviation: 0.1 %

Standard uncertainty: 2.15 Ω

Pooled Degrees of freedom: 3

CALIBRATED VALUE: The tail resistor is calibrated by measuring its resistance with a multimeter. The uncertainty of each calibration is 0.05% (k=2).

R_D:

Type A

Method of observation: Direct

Number of observation: 4

No.	Observation
1	222.47
2	222.47
3	222.52
4	222.56

Arithmetic mean: 222.505 Ω

Pooled Standard deviation: 0.1 %

Standard uncertainty: 0.111 Ω

Pooled Degrees of freedom: 3

CALIBRATED VALUE: The front resistor is calibrated by measuring its resistance with a multimeter. The uncertainty of each calibration is 0.05% (k=2)

C_L:

Type B normal distribution

Value: $30 \cdot 10^{-12}$ F

Expanded uncertainty: $5 \cdot 10^{-12}$ F

Coverage factor: 2

VALUE MEASURED BY USER: The load capacitance is measured by the user using the supplied multimeter. An uncertainty of 5 pF is assumed.

R_L:

Type B normal distribution

Value: $1 \cdot 10^{6}$ Ω

Expanded uncertainty: $10 \cdot 10^3$ Ω

Coverage factor: 2

VALUE MEASURED BY USER: The load resistance is measured by the user using the supplied multimeter. An uncertainty of 1 % is assumed.

U_C:

Type B normal distribution

Value: 1 V

Expanded uncertainty: $200 \cdot 10^{-6}$ V

Coverage factor: 2

MEASURED VALUE: The charging voltage is measured automatically using an HP34401A multimeter. The uncertainty is less than 0.02% (200 ppm).

υ_C:

Type B rectangular distribution

Value: 1.00025

Half-width of distribution: .00025

VOLTAGE COEFFICIENT: The measured quadratic voltage characteristics were approximately quadratic, with a minimum value of 1,0000 and maximum 1,0005. This is modelled as rectangular distribution between these values.

α_C:

Type B rectangular distribution

Value: 0.000000 K^{-1}

Half-width of distribution: 0.000150 K^{-1}

TEMPERATURE COEFFICIENT: The temperature coefficient of the capacitors (NPO ceramic) is +/- 30 ppm/K. Five times this value is taken into this uncertainty estimate.

α_R:

Type B rectangular distribution

Value: 0.000000 K^{-1}

Half-width of distribution: 0.000030 K^{-1}

TEMPERATURE COEFFICIENT: The temperature coefficient of the resistors is +/- 10 ppm/degree according to the specifications. Five times this value is taken into this uncertainty estimate.

ΔT:

Type B rectangular distribution

Value: 0 K

Half-width of distribution: 5 K

TEMPERATURE DIFFERENCE: The difference between the temperatures during calibration and use. Calibration is performed at 22 degrees Celsius.

u_C:

Type B normal distribution

Value: 0

Expanded uncertainty: $250 \cdot 10^{-6}$

Coverage factor: 1

The best estimates of the temperature coefficient and the deviation from the component calibration temperature are zero. Therefore, second order terms must be taken into account in the evaluation of the uncertainty contribution. This uncertainty is the product of standard uncertainties associated with the factors of the product term ($\alpha_C * \Delta T$) in the model equation. This uncertainty is $u_C = 250 \times 10^{-6.}$

u_R:

Type B normal distribution

Value: 0

Expanded uncertainty: $83.3 \cdot 10^{-6}$

Coverage factor: 1

The best estimates of the temperature coefficient and the deviation from the component calibration temperature are zero. Therefore, second order terms must be taken into account in the evaluation of the uncertainty contribution. This uncertainty is the product of standard uncertainties associated with the factors of the product term ($\alpha_R * \Delta T$) in the model equation. The final uncertainty is $u_R = 83.3 \times 10^{-6.}$

Uncertainty budget:

Quantity	Value	Standard uncertainty	Degrees of freedom	Sensitivity coefficient	Uncertainty contribution	Corr.-coeff.	Index
C_S	$18.3918 \cdot 10^{-9}$ F	$23.0 \cdot 10^{-12}$ F	2	$4.01 \cdot 10^{6}$	$92.3 \cdot 10^{-6}$ V	0.46	0.215
C_B	$1.288175 \cdot 10^{-9}$ F	$966 \cdot 10^{-15}$ F	2	$-56.0 \cdot 10^{6}$	$-54.1 \cdot 10^{-6}$ V	-0.27	0.074
R_E	4306.38 Ω	2.15 Ω	3	$3.31 \cdot 10^{-6}$	$7.14 \cdot 10^{-6}$ V	0.04	0.001
R_D	222.505 Ω	0.111 Ω	3	$-65.2 \cdot 10^{-6}$	$-7.25 \cdot 10^{-6}$ V	-0.04	0.001
C_L	$30.00 \cdot 10^{-12}$ F	$2.50 \cdot 10^{-12}$ F	50	$-56.0 \cdot 10^{6}$	-0.000140 V	-0.70	0.496
R_L	$1.00000 \cdot 10^{6}$ Ω	5000 Ω	50	$235 \cdot 10^{-12}$	$1.18 \cdot 10^{-6}$ V	0.01	0.000
U_C	1.000000 V	0.000100 V	50	0.916	$91.6 \cdot 10^{-6}$ V	0.46	0.212
υ_C	1.000250	0.000144	∞	0.00168	$242 \cdot 10^{-9}$ V	0.00	0.000
α_C	0.0 K^{-1}	$86.6 \cdot 10^{-6}$ K^{-1}	∞	0.0	0.0 V	0.0	0.0
α_R	0.0 K^{-1}	$17.3 \cdot 10^{-6}$ K^{-1}	∞	0.0	0.0 V	0.0	0.0
ΔT	0.0 K	2.89 K	∞	0.0	0.0 V	0.0	0.0
u_C	0.0	0.000250	50	0.00168	$420 \cdot 10^{-9}$ V	0.00	0.000
u_R	0.0	$83.3 \cdot 10^{-6}$	50	-0.000235	$-19.6 \cdot 10^{-9}$ V	0.00	0.000
C_{Sx}	$18.3963 \cdot 10^{-9}$ F	$23.6 \cdot 10^{-12}$ F					
C_{Bx}	$1.28850 \cdot 10^{-9}$ F	$1.04 \cdot 10^{-12}$ F					
R_{Ex}	4306.38 Ω	2.18 Ω					
R_{Dx}	222.505 Ω	0.113 Ω					
C_2	$1.31850 \cdot 10^{-9}$ F	$2.71 \cdot 10^{-12}$ F					
d	79.222	0.411					
a	$23.241 \cdot 10^{-6}$	$131 \cdot 10^{-9}$					
b	85.211	0.440					
c	$1.00453 \cdot 10^{6}$	5000					
g	$-3.65450 \cdot 10^{6}$	7250					
h	-11826.9	15.5					
t_P	$1.57394 \cdot 10^{-6}$ s	$2.67 \cdot 10^{-9}$ s					
η	0.915523	0.000176					
U_P	0.915523 V	0.000199 V	31				

Result:

Quantity: U_P

Value: 0.91552 V

Relative expanded uncertainty: ±0.045 %

Coverage factor: 2.1

Coverage probability: 95.45%